

NASA Contract Report No. 194905



# Reciprocity-Based Experimental Determination Of Dynamic Forces and Moments: A Feasibility Study

István L. Vér and Michael S. Howe  
BBN Systems and Technologies

(NASA-CR-194905) RECIPROCITY-BASED  
EXPERIMENTAL DETERMINATION OF  
DYNAMIC FORCES AND MOMENTS: A  
FEASIBILITY STUDY Final Report  
(BBN Systems and Technologies  
Corp.) 72 p

N94-33023

Unclass

G3/71 0009921

NASA Contract No. NAS1-19061

May 1994

National Aeronautics and Space Administration  
Langley Research center  
Hampton, Virginia 23681-0001



REPORT DOCUMENTATION PAGE			Form Approved OMB No. 0704-0188	
Public reporting burden for this collection of information is estimated to average 1 hour per response, including the time for reviewing instructions, searching existing data sources, gathering and maintaining the data needed, and completing and reviewing the collection of information. Send comments regarding this burden estimate or any other aspect of this collection of information, including suggestions for reducing this burden, to Washington Headquarters Services, Directorate for Information Operations and Reports, 1215 Jefferson Davis Highway, Suite 1204, Arlington, VA 22202-4302, and to the Office of Management and Budget, Paperwork Reduction Project (0704-0188), Washington, DC 20503.				
1. AGENCY USE ONLY (Leave blank)		2. REPORT DATE May 1994		3. REPORT TYPE AND DATES COVERED Contractor Report
4. TITLE AND SUBTITLE Reciprocity-Based Experimental Determination of Dynamic Forces and Moments: A Feasibility Study			5. FUNDING NUMBERS Contract NAS1-19061 WU 538-03-14-01	
6. AUTHOR(S) István L. Vér and Michael S. Howe				
7. PERFORMING ORGANIZATION NAME(S) AND ADDRESS(ES) Georgia Institute of Technology Atlanta, GA 30332 BBN Systems and Technologies (Subcontractor) 10 Moulton Street Cambridge, MA 02138			8. PERFORMING ORGANIZATION REPORT NUMBER BBN Report No. 7967 BBN Project No. 621697	
9. SPONSORING / MONITORING AGENCY NAME(S) AND ADDRESS(ES) National Aeronautics and Space Administration Langley Research Center Hampton, VA 23681-0001			10. SPONSORING / MONITORING AGENCY REPORT NUMBER NASA CR-194905	
11. SUPPLEMENTARY NOTES Langley Technical Monitor: Kevin P. Shepherd Task 7 Final Report prepared by BBN Systems and Technologies for Georgia Tech under subcontract no. A-8612-S1.				
12a. DISTRIBUTION / AVAILABILITY STATEMENT Unclassified — Unlimited Subject Category — 71			12b. DISTRIBUTION CODE	
13. ABSTRACT (Maximum 200 words) BBN Systems and Technologies has been tasked by the Georgia Tech Research Center to carry Task Assignment No. 7 for the NASA Langley Research Center to explore the feasibility of "In-Situ Experimental Evaluation of the Source Strength of Complex Vibration Sources Utilizing Reciprocity." The task was carried out under NASA Contract No. NAS1-19061.  In flight it is not feasible to connect the vibration sources to their mounting points on the fuselage through force gauges to measure dynamic forces and moments directly. However, it is possible to measure the interior sound field or the vibration response caused by these structureborne sound sources at many locations and invoke the principle of reciprocity to predict the dynamic forces and moments. The work carried out in the framework of Task 7 was directed to explore the feasibility of reciprocity-based measurements of vibration forces and moments.				
14. SUBJECT TERMS Noise; Vibration; Interior Noise			15. NUMBER OF PAGES Text: 48 Appendices: 14	
			16. PRICE CODE	
17. SECURITY CLASSIFICATION OF REPORT Unclassified	18. SECURITY CLASSIFICATION OF THIS PAGE Unclassified	19. SECURITY CLASSIFICATION OF ABSTRACT Unclassified	20. LIMITATION OF ABSTRACT	

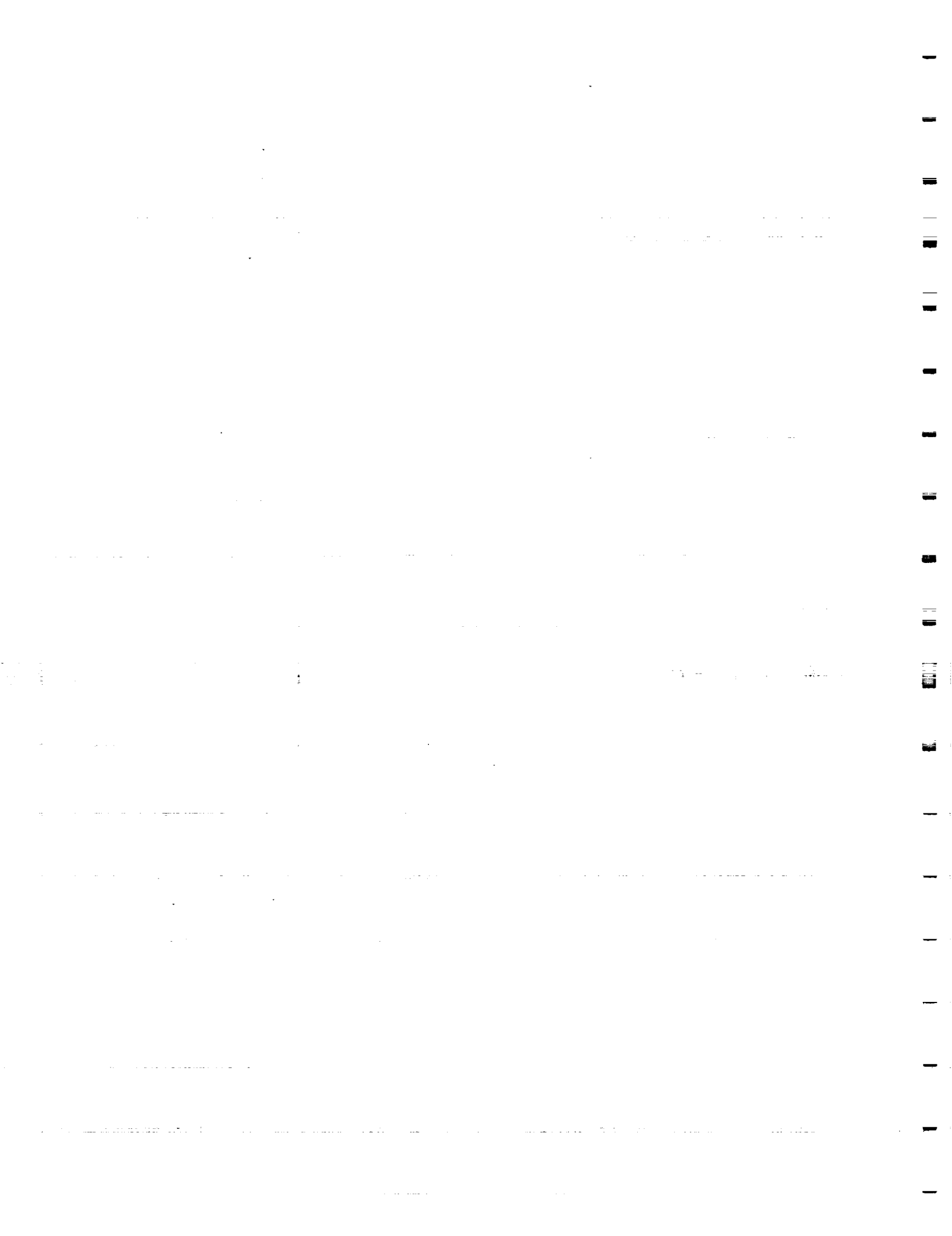


## TABLE OF CONTENTS

	Page
REPORT DOCUMENTATION PAGE .....	iii
TABLE OF CONTENTS .....	v
LIST OF FIGURES .....	vii
LIST OF TABLES .....	ix
SUMMARY AND CONCLUSIONS .....	1
1. FORMULATIONS OF RECIPROCITY .....	2
1.1 Reciprocity Prediction of Interior Noise Due to Dynamic Force and Moment Excitation .....	3
1.2 Experimental Determination of the Excitation Forces and Moments Through a Combination of Non-Intrusive Direct and Reciprocal Measurements .....	4
1.3 Simultaneous Multiple Input .....	6
1.4 Advantages and Disadvantages of the Different Reciprocity Methods .....	9
1.5 Effect of Redundancy on Prediction Accuracy .....	11
2. RECIPROCITY TRANSDUCERS .....	11
2.1 Design Goals .....	11
2.2 Design of the Reciprocity Transducers .....	12
<i>Large Reciprocity Transducer</i> .....	12
<i>Checkout</i> .....	15
<i>Small Reciprocity Transducer</i> .....	17

TABLE OF CONTENTS (cont'd)

	Page
3. RECIPROCITY EXPERIMENTS.....	23
3.1 Test Article .....	23
3.1 Two Force Excitation .....	25
3.2 Moment Excitation .....	42
REFERENCES .....	48
APPENDIX A: Sensitivity Analysis of the Redundancy on Prediction Accuracy .....	A-1
APPENDIX B: Construction Drawings for the Large Pentatondodecahedron Transducer .....	B-1
APPENDIX C: Construction Drawings for the Small Pentatondodecahedron Transducer .....	C-1

## LIST OF FIGURES

	Page
1. Determination of In-Flight Forces $\bar{F}_1$ and $\bar{F}_2$ Utilizing Reciprocity .....	7
2. Photograph of the Large Perntatondodecahedron Transducer .....	13
3. Wiring Diagram of the 12 Woofers in the Large Pentatondodecahedron Transducer .....	14
4. Magnitude and Phase of the Electrical Impedance, $Z=U_L/i$ , Measured for a Large Pentatondodecahedron Transducer. ....	16
5. Volume Acceleration vs. Excitation Voltage Calibration Curve of a Large Pentatondodecahedron Transducer .....	18
6. Volume Acceleration vs. Excitation Current Calibration Curve of a Large Pentatondodecahedron Transducer .....	19
7. Linearity Check; Sound Pressure Level at 1 Meter Minus Loudspeaker Excitation Voltage Level Obtained for 1 Volt and 10 Volt Loudspeaker Voltage .....	20
8. Directionality Check; Transfer Function (Microphone Voltage/Loudspeaker Voltage) Measured at 10 Degree Incremental Rotation of the Large Transducer .....	21
9. Photograph of the Small Pentatondodecahedron Transducer .....	22
10. Directivity Check; Transfer Function (Microphone Voltage/Loudspeaker Voltage) Measured at 10 Degree Incremental Rotation of the Small Transducer .....	24
11. Sketch of the Fuselage Model Identifying Excitation Positions 1 and 2 and Receiver Positions A, B, C and D .....	26
12. Direct Transfer Function $v_{A1}/F_1$ and Corresponding Reciprocal Transfer Function $U_{1A}/i_A$ .....	29

FIGURES (cont'd)	Page
13. Direct Transfer Function $U_{B1}/F_1$ and Corresponding Reciprocal Transfer Function $v_{1B}/i_B$ .....	30
14. Direct Transfer Function $U_{C1}/F_1$ and Corresponding Reciprocal Transfer Function $v_{1C}/i_C$ .....	31
15. Direct Transfer Function $U_{D1}/F_1$ and Corresponding Reciprocal Transfer Function $v_{1D}/i_D$ .....	32
16. Direct Transfer Function $U_{A2}/F_2$ and Corresponding Reciprocal Transfer Function $v_{2A}/i_A$ .....	33
17. Direct Transfer Function $U_{B2}/F_2$ and Corresponding Reciprocal Transfer Function $v_{2B}/i_B$ .....	34
18. Direct Transfer Function $U_{C2}/F_2$ and Corresponding Reciprocal Transfer Function $v_{2C}/i_C$ .....	35
19. Direct Transfer Function $U_{D2}/F_2$ and Corresponding Reciprocal Transfer Function $v_{2D}/i_D$ .....	36
20. Driving Point Input and Response Characteristics, Excitation Pos. 1 Transducer Location C .....	37
21. Change in Force Spectra due to Successive Reattachments of the Shaker/Force Gauge Assembly at Excitation Position 1 .....	38
22. Comparison of the Directly Measured Transfer Function $U_{C1}/F_{1C}$ with Reciprocity Prediction $v_{1C}/i_{C1}$ .....	39
23. Coherence Functions .....	40
24. Effect of Averaging on Reciprocity Prediction; Force Excitation at Pos. 1; Transducer Locations A, B, C and D .....	43
25. Input Accelerance at Excitation Point 2 .....	44



FIGURES (cont'd)	Page
26. Change in Force Spectra due to Successive Reattachments of the Shaker/Force Gauge Assembly at Excitation Point 2 .....	45
27. Prediction of Force $\tilde{F}_2$ Utilizing Reciprocity .....	46
28. Comparison of the Direct and Reciprocal Transfer Function Obtained for Moment Excitation.....	47

## LIST OF TABLES

Table 1: Reciprocity Relationships For Single Point Force And Moment Excitation.....	3
Table 2: Prediction Of An Unknown Force Of Moment Invoking Reciprocity .....	5

## SUMMARY AND CONCLUSIONS

BBN Systems and Technologies\* (BBN) has been tasked by the Georgia Tech Research Center (Georgia Tech) to carry out Task Assignment #7 for the NASA Langley Research Center (NASA Langley) to explore the feasibility of "In-Situ Experimental Evaluation of the Source Strength of Complex Vibration Sources Utilizing Reciprocity. The Task was carried out under NASA Contract No. NAS 1-19061.

In flight it is not feasible to connect the vibration sources to their mounting points on the fuselage through force gauges to measure dynamic forces and moments directly. However, it is possible to measure the interior sound field or the vibration response caused by these structureborne sound sources at many locations and invoke the principle of reciprocity to predict the dynamic forces and moments. The work carried out in the framework of Task 7 was directed to explore the feasibility of reciprocity-based measurements of vibration forces and moments. The work performed included:

1. analytical extension of the principle of reciprocity to deal with a moment and multiple forces,
2. design, manufacture and performance checkout of two reciprocity transducers,
3. assistance to NASA Langley in carrying out specific reciprocity experiments utilizing the special transducers, and
4. analysis of the experimental data obtained by NASA Langley.

The key results of the work carried out in Task 7 were :

1. a pentatondodecahedron-shaped reciprocity transducer that in its transmitter mode of operation works as an omni-directional loudspeaker and in its receiver mode as an omni-directional

---

\* a division of Bolt Beranek and Newman Inc.

microphone. The transducer is powerful enough to generate sufficient signal/noise ratio in measuring the sound-induced vibration of a typical fuselage in the reciprocal experiments and sensitive enough to yield sufficient signal noise/ratio in sensing the interior sound field in the direct experiments;

2. a new, formulation of the reciprocity principle (which does not require the volume velocity calibration of the transducer) and lends itself much better for the in-situ measurements of dynamic forces and moments than traditional reciprocity methods;
3. the analysis of limited experimental data collected indicates that further improvement in the vibration response measurements techniques will be needed to yield sufficient accuracy for the reciprocal measurements of moments. The needed improvements are within the capabilities of current signal processing and transducer technology;
4. reciprocity techniques for vibroacoustic calibration of aircraft fuselages and for non-intrusive, indirect measurement of vibration forces and moments are promising to warrant further investigations.

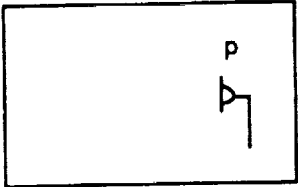
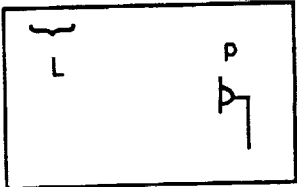
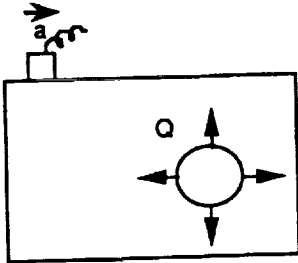
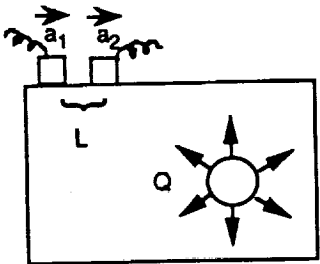
## 1. FORMULATIONS OF RECIPROCITY

To predict accurately the structureborne component of the interior noise and to optimize measures to reduce it, it is necessary to know the magnitude and phase of the dynamic forces,  $F$ , and moments,  $M$ , acting on the fuselage and to know the magnitude and phase of the transfer functions  $p/F$  and  $p/M$  describing the relationship between the sound pressure,  $p$ , in the fuselage and the forces and moments which cause it. Reciprocity as an experimental tool can be used for accomplishing both of these tasks. The ways reciprocity is used are briefly discussed below.

### 1.1 Reciprocity Prediction of Interior Noise Due to Dynamic Force and Moment Excitation

Previous work carried out under NASA sponsorship have dealt with the reciprocity prediction of aircraft interior noise due to point force inputs [1, 2]. Considering moment  $M=FL$  as the superposition of two forces,  $F$ , of equal magnitude and opposing phase acting at a distance  $L$  apart, the reciprocity relationship for moment excitation also can be derived [3]. These reciprocity relationships are compiled in Table 1 below.

**TABLE 1**  
**RECIPROCITY RELATIONSHIPS FOR SINGLE**  
**POINT FORCE AND MOMENT EXCITATION**

Force Excitation	Moment Excitation
$P / \bar{F} = \frac{\bar{a} / j\omega}{Q}$	$P / \bar{M} = \frac{(\bar{a}_1 - \bar{a}_2) / j\omega L}{Q}$
<p><math>\downarrow \bar{F}</math></p>  <p>Direct</p>	<p><math>F \downarrow \uparrow F</math> <span style="float: right;"><math>\bar{M} = FL</math></span></p>  <p>Direct</p>
 <p>Reciprocal</p>	 <p>Reciprocal</p>

In Table 1 the symbols are defined as follows:

$\vec{F}$  = Point force excitation

$p$  = Sound pressure response at the receiver location caused by force  $F$  or Moment  $M=FL$

$\vec{a}$  = acceleration response at the former excitation point caused by point sound source of volume velocity  $Q$  located at the former receiver location; acceleration is measured in the same direction as the formerly applied force

$Q$  = Volume velocity of the point sound source

$j = \sqrt{-1}$

$\omega = 2\pi f$  = angular frequency

$L$  = distance between the accelerometers measuring the acceleration response difference  $\vec{a}_1 - \vec{a}_2$ ;  $(\vec{a}_1 - \vec{a}_2) / j\omega L$  is the angular velocity response

The arrows above the symbols signify that they are vector quantities.

## 1.2 Experimental Determination of the Excitation Forces and Moments Through a Combination of Non-Intrusive Direct and Reciprocal Measurements

During the framework of this task we have also developed a new non-intrusive measurement method for in-situ determination of a force or moment acting on the fuselage structure. Both the new and the originally proposed reciprocity relationships are summarized in Table 2. In Table 2 the symbol  $U_{oc}$  represents the open circuit voltage of the reciprocity transducer operating at its receiver mode and  $i$  the current through the transducer when operating in its transmitter mode.

TABLE 2  
PREDICTION OF AN UNKNOWN FORCE  
OR MOMENT INVOKING RECIPROCITY

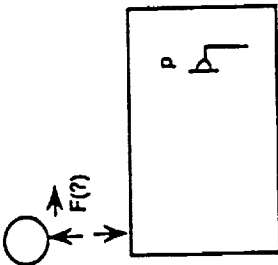
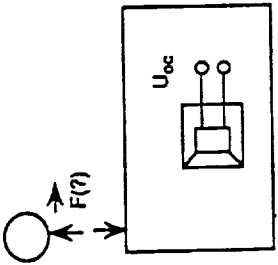
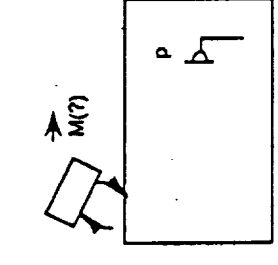
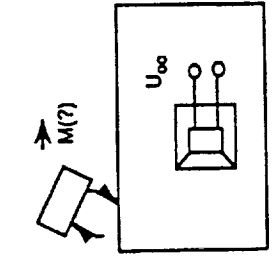
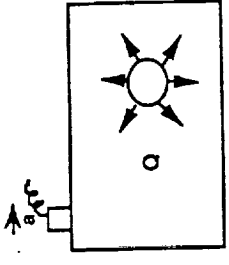
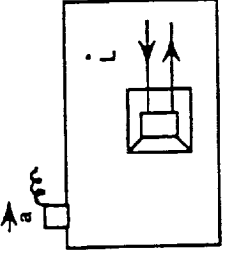
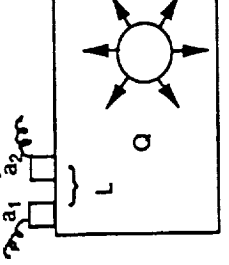
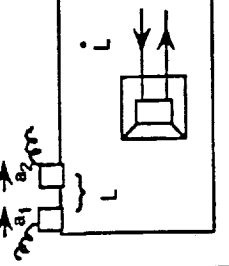
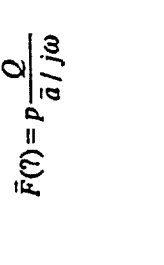
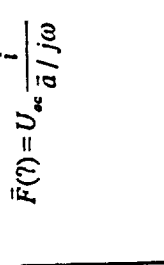
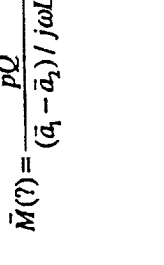
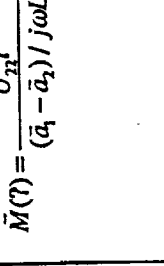
	FORCE PREDICTION METHOD		MOMENT PREDICTION	
	Originally Proposed	Improved	Originally Proposed	Improved
Direct Listening				
Reciprocal				
Non-Intrusive				
Prediction	$\bar{F}(\gamma) = p \frac{Q}{\bar{a}} / j\omega$	$\bar{F}(\gamma) = U_{\infty} \frac{i}{\bar{a}} / j\omega$	$\bar{M}(\gamma) = \frac{pQ}{(\bar{a}_1 - \bar{a}_2) / j\omega L}$	$\bar{M}(\gamma) = \frac{U_{\infty} i}{(\bar{a}_1 - \bar{a}_2) / j\omega L}$

Table 2 contains two prediction methods labeled as "originally proposed" and "improved" respectively. The *originally proposed method* employs an omni-directional microphone as a receiver while performing the direct, non-intrusive "direct listening" experiment and an omni-directional point sound source of known volume velocity calibration while performing the "reciprocal sound excitation" experiments. As noticed during preliminary experiments, the *originally proposed method* had the disadvantages of requiring (1) volume velocity calibration of the sound source, (2) determination of the acoustic center of the sound source, (3) exact placement of the acoustic center at the former microphone position, (4) omni-directional radiation characteristics of the source. These requirements made it unduly difficult to obtain accurate predictions at high frequencies.

To overcome these difficulties we have developed the *improved method* (see Table 2). Here the same transducer is used for the "direct listening" and the "reciprocal sound excitation" measurements; first as a microphone and then as a sound source. No acoustic calibration of the transducer is required. The transducer does not need to be omni-directional. The open circuit voltage  $U_{oc}$  and the current through the transducer,  $i$ , can be measured with high accuracy.

### 1.3 Simultaneous Multiple Input

The analytical basis for measuring simultaneous multiple excitation is illustrated in this section by considering the simple case of two dynamic forces  $F_1$  and  $F_2$  which act simultaneously on the fuselage structure at engine mounting points 1 and 2 respectively, as depicted in Fig 1A. These two unknown vertical forces produce the vibration velocity responses  $v_{31}$  and  $v_{41}$  or acoustic response in form of open circuit voltage of the reciprocity transducer  $U_3$  and  $U_4$  at locations 3 and 4. These responses are recorded simultaneously in flight.

Before the flight test or after it, on the ground, the fuselage is excited by forces  $F_3$  and  $F_4$  or the acoustic volume within the fuselage is energized by sending current  $i_3$  and  $i_4$  through the reciprocity transducers. The velocity response  $v_{13}$ ,  $v_{23}$ ,  $v_{14}$  and  $v_{24}$  is recorded at the former excitation points in the form of the transfer functions  $v_{13}/F_3$ ,  $v_{23}/F_3$ ,  $v_{14}/F_4$ ,  $v_{24}/F_4$  for secondary force excitation or in form of  $v_{13}/i_3$ ,  $v_{23}/i_3$ ,  $v_{14}/i_4$ ,  $v_{24}/i_4$  as shown in Fig 1B and 1C.

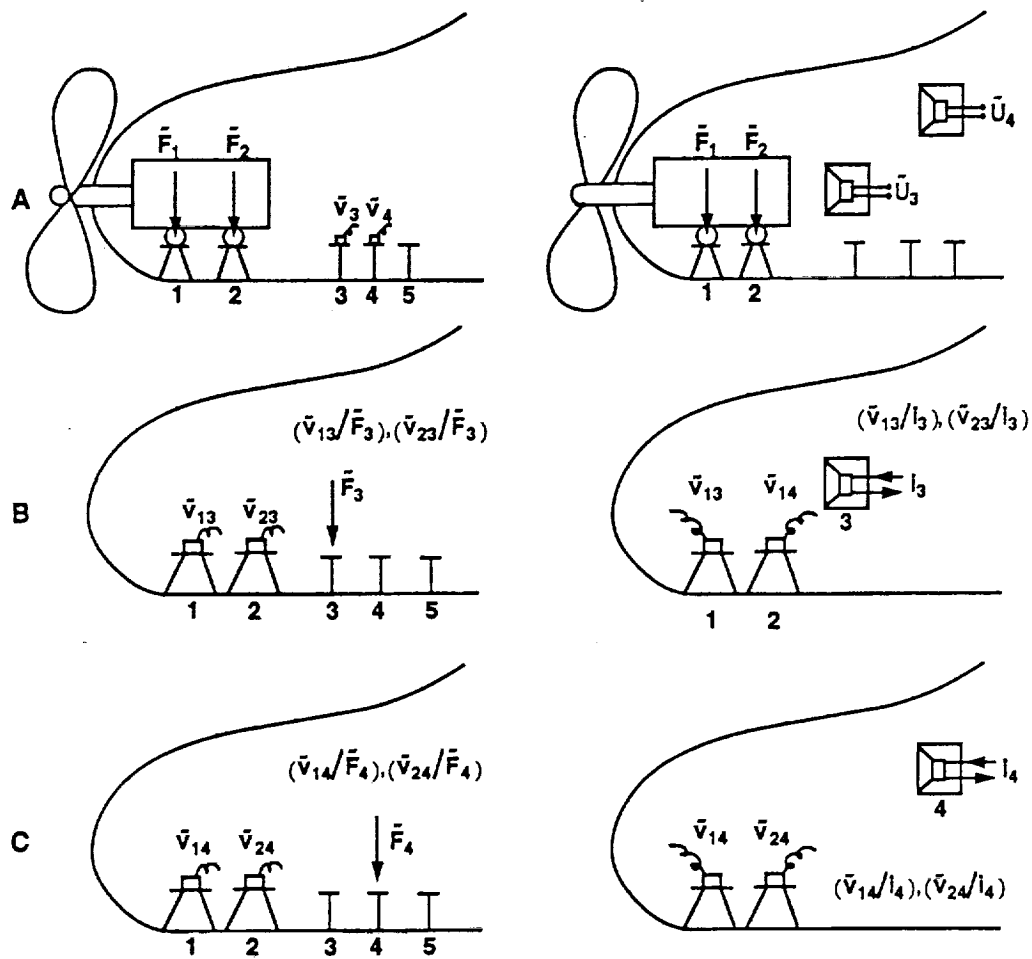


Fig. 1. Determination of In-Flight Forces  $\bar{F}_1$  and  $\bar{F}_2$  Utilizing Reciprocity

- A. In-flight, record responses  $\bar{v}_3, \bar{v}_4$  or  $\bar{U}_3, \bar{U}_4$  due to unknown forces  $\bar{F}_1$  and  $\bar{F}_2$ .
- B. On ground, apply excitation  $\bar{F}_3$  or  $i_3$  and record responses  $\bar{v}_{13}$  and  $\bar{v}_{23}$ .
- C. On ground, apply excitation  $\bar{F}_4$  or  $i_4$  and record responses  $\bar{v}_{14}$  and  $\bar{v}_{24}$ .



During these reciprocal experiments the former excitation point 1 and 2 must be unrestrained by disconnecting them from the structure from which they receive the force excitation during flight (e.g. disconnecting\* the engine from its mounts). If the reciprocal experiments employ Forces  $\bar{F}_3, \bar{F}_4$ , as shown on the left side of Figs 1B and 1C, the two unknown forces  $\bar{F}_1$  and  $\bar{F}_2$  are determined from the following equations:

$$\bar{v}_3 = \bar{F}_1(\bar{v}_{31} / \bar{F}_1) + \bar{F}_2(\bar{v}_{32} / \bar{F}_2) \quad (1a)$$

$$\bar{v}_4 = \bar{F}_1(\bar{v}_{41} / \bar{F}_1) + \bar{F}_2(\bar{v}_{42} / \bar{F}_2) \quad (1b)$$

Since the direct transfer functions in equations 1a and 1b are not known, we replace them with their reciprocal counterparts [1,2] given by:

$$(\bar{v}_{31} / \bar{F}_1) = (\bar{v}_{13} / \bar{F}_3) \quad (2a)$$

$$(\bar{v}_{32} / \bar{F}_2) = (\bar{v}_{23} / \bar{F}_3) \quad (2b)$$

$$(\bar{v}_{41} / \bar{F}_1) = (\bar{v}_{14} / \bar{F}_4) \quad (2c)$$

$$(\bar{v}_{42} / \bar{F}_2) = (\bar{v}_{24} / \bar{F}_4) \quad (2d)$$

This yields:

$$\bar{v}_3 = \bar{F}_1(\bar{v}_{13} / \bar{F}_3) + \bar{F}_2(\bar{v}_{23} / \bar{F}_3) \quad (3a)$$

$$\bar{v}_4 = \bar{F}_1(\bar{v}_{14} / \bar{F}_4) + \bar{F}_2(\bar{v}_{24} / \bar{F}_4) \quad (3b)$$

Equations 3a and 3b can be solved for the sought excitation forces  $F_1$  and  $F_2$  yielding:

$$\bar{F}_1 = \left[ \frac{\bar{F}_3(\bar{v}_3 / \bar{v}_{23}) - \bar{F}_4(\bar{v}_4 / \bar{v}_{24})}{(\bar{v}_{13} / \bar{v}_{23}) - (\bar{v}_{14} / \bar{v}_{24})} \right] \quad (4a)$$

$$\bar{F}_2 = \left[ \frac{\bar{F}_4(\bar{v}_4 / \bar{v}_{14}) - \bar{F}_3(\bar{v}_3 / \bar{v}_{13})}{(\bar{v}_{24} / \bar{v}_{14}) - (\bar{v}_{23} / \bar{v}_{13})} \right] \quad (4b)$$

Inspection of equations 4a and 4b, shows that both the numerator and denominator are in the form of a difference. Consequently, at those particular

\* It is expedient to perform the reciprocal experiments first, before the engine is mounted.

frequencies where either the numerator or the denominator are very small, the possibility of a sizable error may occur, due to measurement inaccuracy. Consequently, redundancy (by using a few more shaker excitation locations than the number of active excitation locations) is advisable.

If the reciprocal experiments employ acoustic excitation, as shown on the right side of Figs 1B and 1C, the force prediction equations takes the form

$$\tilde{F}_1 = \left[ \frac{\tilde{i}_3(\tilde{U}_3 / \tilde{v}_{23}) - \tilde{i}_4(\tilde{U}_4 / \tilde{v}_{24})}{(\tilde{v}_{13} / \tilde{v}_{23}) - (\tilde{v}_{14} / \tilde{v}_{24})} \right] \quad (5a)$$

$$\tilde{F}_2 = \left[ \frac{\tilde{i}_4(\tilde{U}_4 / \tilde{v}_{14}) - \tilde{i}_3(\tilde{U}_3 / \tilde{v}_{13})}{(\tilde{v}_{24} / \tilde{v}_{14}) - (\tilde{v}_{23} / \tilde{v}_{13})} \right] \quad (5b)$$

The analysis presented here was carried out for only two simultaneously acting vertical forces. If there are  $n$  simultaneously acting forces, each with three orthogonal components,  $x$ ,  $y$ ,  $z$ , then we would need a minimum of  $n$  shaker locations where the fuselage is excited in the  $x$ ,  $y$ , and  $z$  directions (i.e., by mounting a small cube-shaped metal block at each location and using this for the mounting of the accelerometers and the shakers) or using  $3n$  acoustical excitation locations. In both cases, we would have  $3n$  linear equations such as Equations 3a, 3b or 5a and 5b which can be solved for the  $3n$  or orthogonal components of the  $n$  simultaneously acting forces.

#### 1.4 Advantages and Disadvantages of the Different Reciprocity Methods

As shown in the left and right hand side of Fig. 1, the reciprocal transfer functions can be obtained either by force excitation or by acoustical excitation. The advantages and disadvantages of each mode of obtaining the reciprocal transfer functions are discussed below.

##### *Force Excitation*

As shown on the left-hand-side of Fig. 1, the reciprocal transfer functions  $\tilde{v}_{13} / \tilde{F}_3$ ,  $\tilde{v}_{23} / \tilde{F}_3$ ,  $\tilde{v}_{14} / \tilde{F}_4$  and  $\tilde{v}_{24} / \tilde{F}_4$ , are obtained by applying the known forces  $\tilde{F}_3$  and  $\tilde{F}_4$  by a shaker. These experiments are difficult, cumbersome, and frequently not sufficiently accurate. The reasons for this are:

- a. It takes a long time to mount a shaker and change its position and orientation.
- b. Simultaneously attaching many shakers and leaving them inactive (except one) changes the dynamics of the structure, and therefore is not permissible.
- c. The need to change shaker location or orientation after each set of vibration response measurements precludes the automatization of the experiment.
- d. Frequently, there is not enough space available in the vicinity of many excitation points to accommodate the shaker and force gauge.
- e. Accurate measurement of the force acting on the excitation point is difficult because the inertia of the mounting mass (needed for fastening the force gauge to the structure) is as large or larger than the input impedance of the fuselage. This is usually the case at the frequency of structural resonances where input impedance is controlled by structural damping.

#### *Acoustic Excitation*

As shown on the right-hand-side of Fig. 1, the reciprocal transfer functions  $\bar{v}_{13} / i_3$ ,  $\bar{v}_{23} / i_3$ ,  $\bar{v}_{14} / i_4$  and  $\bar{v}_{24} / i_4$  are obtained by actuating the reciprocity transducer as a loudspeaker by forcing the current  $i_3$  or  $i_4$  through it. This experiment is simpler than the force excitation experiment because:

- a. no shaker is required
- b. no force measurement is required
- c. the reciprocity transducer can be moved more easily than the shaker

## 1.5 Effect of Redundancy on Prediction Accuracy

A sensitivity analysis was carried out to assess the effect of redundancy\* on the prediction of unknown excitation forces or moments. The analyses is presented in Appendix A. The error in determining excitation strength in the presence of noise is represented in the form of normalized mean square error  $\epsilon^2$  in measuring the true force-velocity products. The analyses indicates that the error is proportional to  $\epsilon/(3M)^{1/2}$ , where M is the number of observation and reciprocal excitation locations. M must be greater than the number of unknown excitation forces, N.

## 2. RECIPROCITY TRANSDUCERS

This section deals with the design goals, the design, manufacturing and checkout of two pentatondodecahedron shaped reciprocity transducers.

### 2.1 Design Goals

The design goals for the reciprocity transducer were:

- a. should work as a transmitter as well as a receiver.
- b. should be linear.
- c. in its transmitting mode of operation should be able to produce enough sound power output to produce high sound-induced vibration on the fuselage to yield sufficient signal/noise ratio.
- d. in its receiver mode of operation should have high enough sensitivity to yield sufficient signal/noise ratio.
- e. should be small.
- f. should have an omni-directional radiation and receiver characteristics.
- g. should have a well defined acoustic center.

---

\* more observation points and more reciprocal excitation locations than the number of unknown forces or force components.

---

The actual design, described in the following sections represents a balanced compromise between these conflicting design goals.

## 2.2 Design of the Reciprocity Transducers

This section contains a brief description of the design and performance checkout of the two reciprocity transducers.

### *Large Reciprocity Transducer*

The large pentatondodecahedron-shaped reciprocity transducer is shown in Fig. 2. The geometry of the transducer is documented in BBN Drawings AA02001A, AA02100A, AA02101A, AA02102A, AA02103A and AA02104A presented in Appendix B.

The 12 moving coil loudspeakers constituting the transducer are 4-inch diameter moving coil woofers, Model 206-0408, manufactured by the Analog and Digital Systems Corporation (ADS) in Wilmington, Massachusetts. These woofers were designed for hi-fi automotive applications providing high stroke and low distortion. Their electro-acoustics characteristics are as follows:

Coil Resistance	: 3 Ohm
Bl	: 4 Tesla x meter
Effective Coil Surface Area	: $5.6 \times 10^{-3} \text{ m}^2$
Free Field Resonance Frequency	: 60 Hz
Total Moving Mass	: 5 grams
Mech. Suspension Compliance	: 1300 $\mu\text{m}/\text{Newton}$
Max. Peak Coil Displacement	: $\leq 2.5 \text{ mm}$
Max. Cont. Voltage Allowed	: 10 $V_{\text{eff}}$

Figure 3 shows the wiring diagram of the 12 woofers constituting the active part of the pentatondodecahedron transducer. The series combination of four loudspeaker groups, where each group has 3 loudspeakers wired parallel, yields an  $R=4$  Ohm nominal resistance for the transducer.

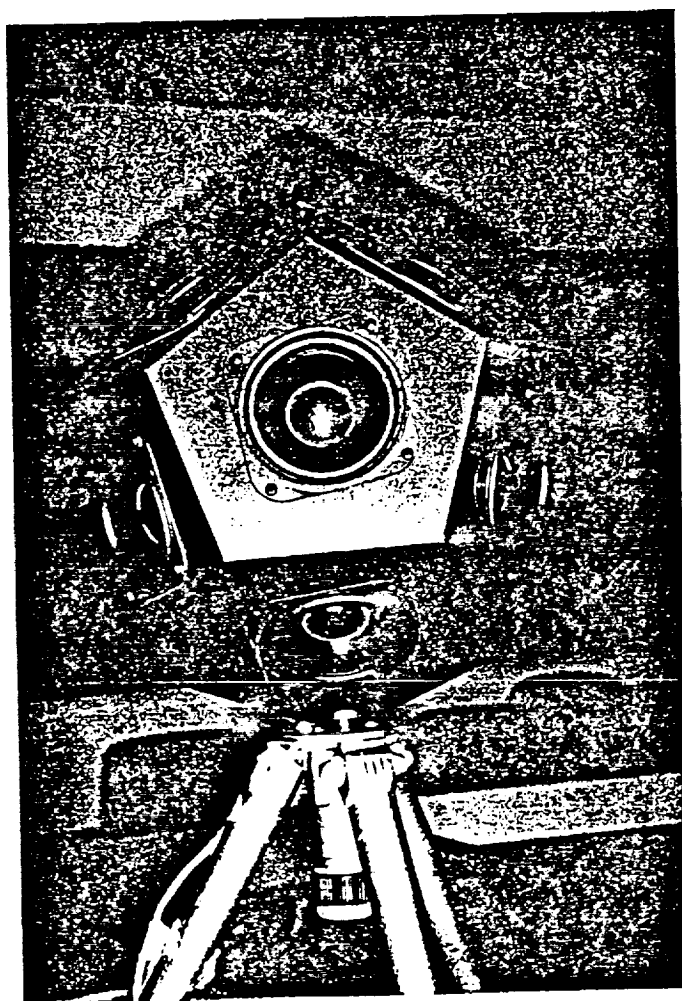
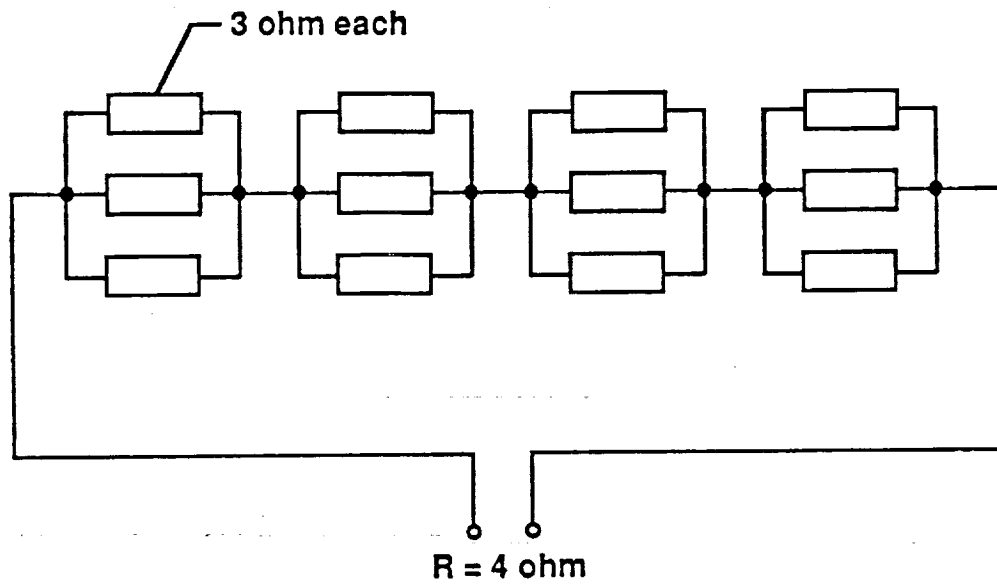


Fig. 2 Photograph of the Pentatondodecahedron Transducer

OUTSIDE RADIUS : 7 INCH ( 178 mm )

INSIDE DIAMETER : 5.47 INCH ( 141.5 mm )



**Figure 3. Wiring Diagram of the 12 Woofers in the Pentatondodecahedron Transducer**

*Checkout*

After the transducer housing was manufactured the loudspeakers were installed, wired and the completed transducer was checked out for proper polarity, electrical impedance, linearity and for the effect of acoustic loading on the volume acceleration.

It was found that all the 12 loudspeakers were moving in phase, the transducer in its transmitter mode of operation was found linear up to  $U_L = 5V_{eff}$  pure tone excitation in the entire frequency range from 100 Hz to 5kHz. Figure 4 shows measured frequency dependence of the transducer's electric impedance  $Z = U_L/i$ . As expected, the magnitude of the electric impedance peaks at the 156 Hz mechanical resonance frequency of the transducer set by the combined inertia of the moving parts of the speakers and stiffness impedance of the air volume of the pentatondodecahedron enclosure. At this resonance frequency the voice coil movement is vigorous and the back-electric voltage,  $Blv$ , induced by the coil movement is in such a phase that it tends to reduce current through the coil and thereby increase the electric resistance.

The large pentatondodecahedron monopole transducer is equipped with a microphone holder that allows the positioning of a 1/4 in diameter Bruel and Kjaer microphone, Model 4135 or 4136 so that the membrane of the microphone is at the geometric center of the interior volume. The purpose of this microphone was to demonstrate that changes of acoustic loading have negligible effect on the volume velocity of the transducer. Preliminary experiments performed at BBN showed that change in acoustic loading, caused by the vicinity of hard surfaces, had negligible effects on the volume velocity output. Consequently, the interior microphone is not needed. We recommend that NASA either should keep the 1/4-inch microphone permanently installed to monitor the functionality of the transducer or the opening for the microphone should be sealed.



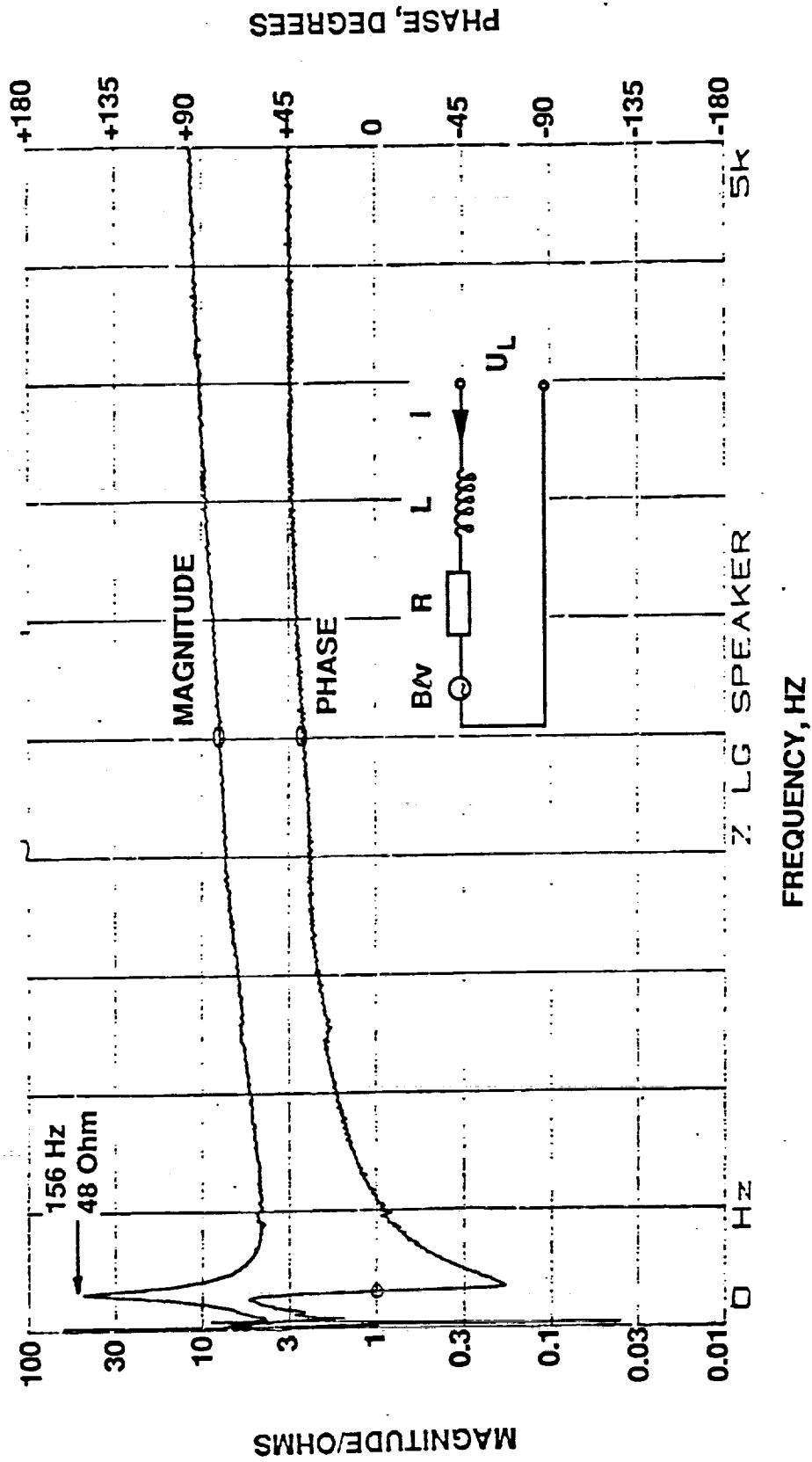


Figure 4. Magnitude and Phase of the Electrical Impedance,  
 $Z = U_L / I$ , Measured for the Pentatondodecahedron  
 Transducer

Figures 5 and 6 show the volume acceleration calibration of a large transducer of nominally identical construction as that delivered to NASA. As shown in Fig. 5 the transducer, operating in its transmitting mode, produces  $1 \text{ m}^3/\text{sec}^2$  to  $5 \text{ m}^3/\text{sec}^2$  volume acceleration\* for 1 volt excitation voltage. According to Fig. 6 the volume acceleration output is about  $1 \text{ m}^3/\text{sec}^2$  for one ampere excitation current.

Figure 7 shows the transfer function  $\text{SPL}(1 \text{ meter}) - \text{dBV}_L$  as a function of frequency from 50 Hz to 5 kHz, where  $\text{SPL}(1 \text{ meter})$  is the sound pressure level (in dB re  $20 \mu\text{Pa}$ ) and  $\text{dBV}_L$  is the excitation voltage level (dB re 1 volt) of the loudspeaker. The two curves were obtained for 1 volt and 10 volt loudspeaker voltage, respectively. Figure 7 indicates that the large transducer is linear and that it produces 90 dB to 100 dB sound pressure level at 1 meter distance for 1 volt excitation voltage.

Figure 8 shows the transfer function between microphone voltage and loudspeaker excitation voltage obtained by NASA at 1m microphone distance. The superimposed transfer functions were obtained by rotating the transducer in 10 degree increments. The close clustering of the curves in Fig. 7 indicates that the transducer has an essentially omni-directional sound radiation characteristics up to 1300 Hz.

#### *Small Reciprocity Transducer*

The small pentatondodecahedron-shaped reciprocity transducer is shown in Fig 9. The geometry of the transducer is documented in BBN Drawings AA02200, AA02201 and AA02202, presented in Appendix C.

The small transducer has a solid pentatondodecahedron-shaped body with a circumradius of 2.627 inches and an inradius of 2.088 inches. The 12 Type 206-0127 tweeters, manufactured by the ADS Corporation, are surface mounted on the solid body. The tweeters have a 1 inch diameter, half-cone-shaped membrane. Each self contained tweeter, with its magnet and back air volume, is mounted on a 2 inch diameter disk which is mounted on each face of the solid body.

---

\* Volume acceleration =  $j \omega Q$ , where  $Q$  is the volume velocity.

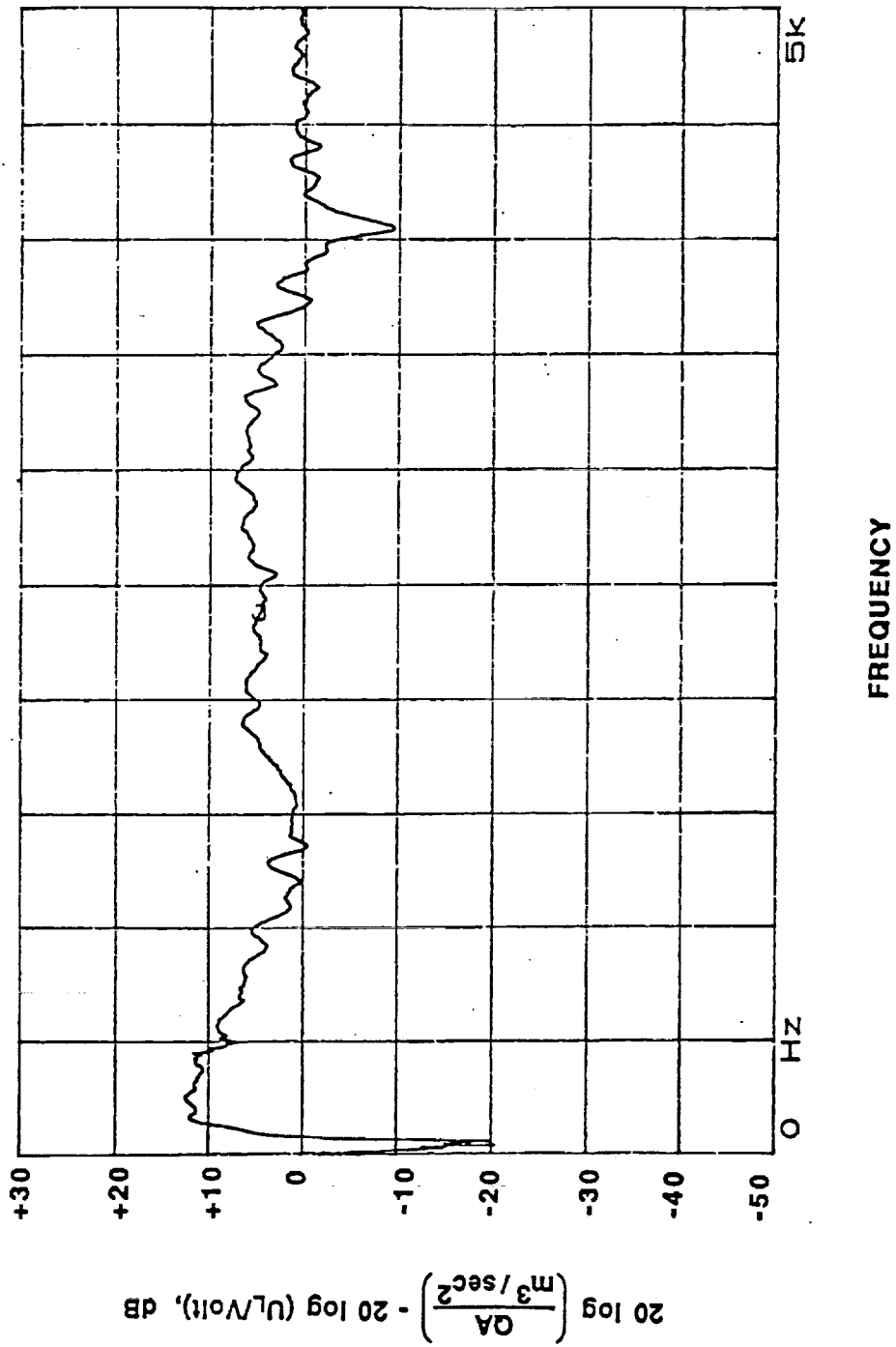


Fig. 5. Volume Acceleration vs. Excitation Voltage Calibration Curve of a Large Pentatondodecahedron Transducer.

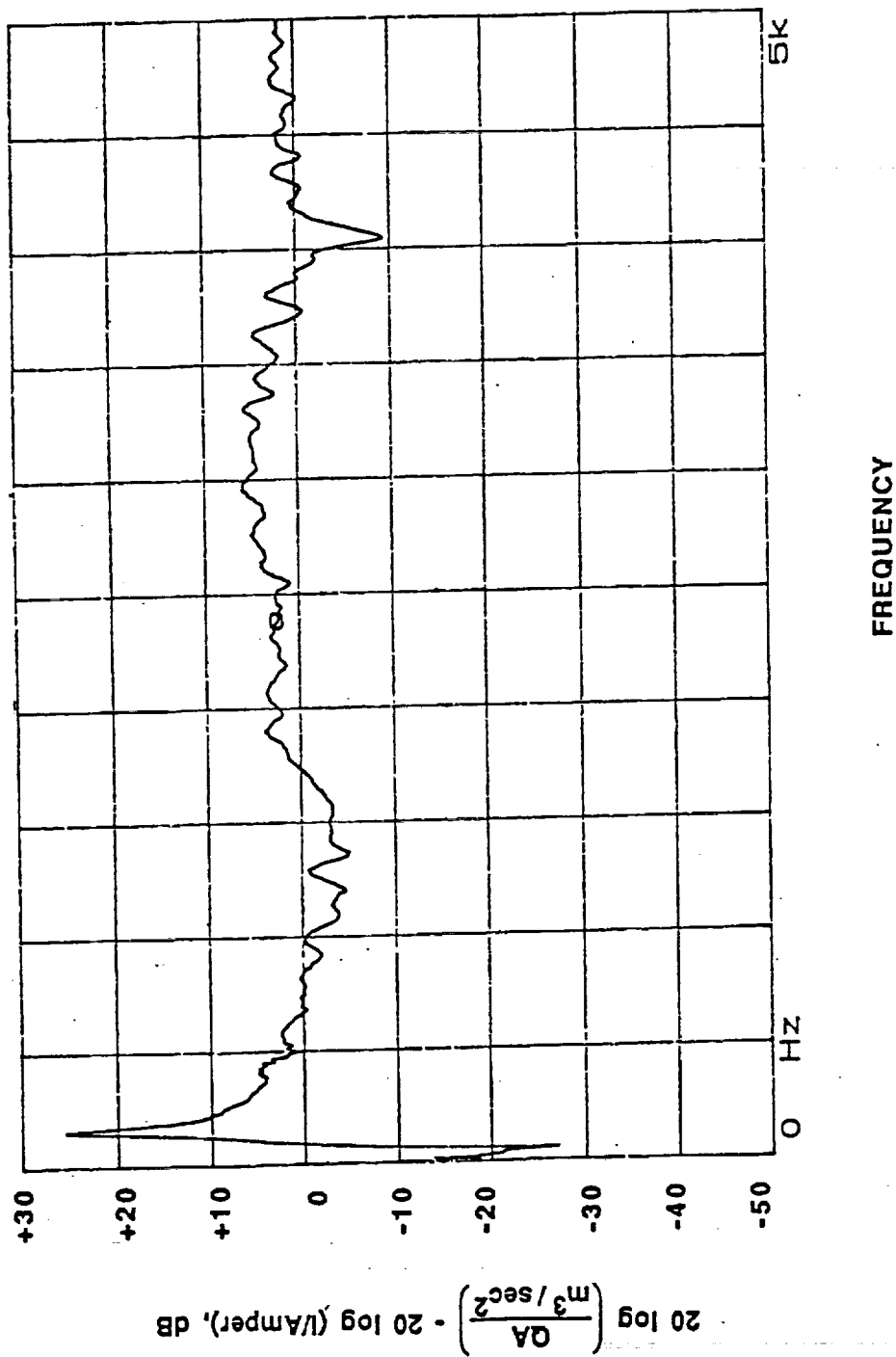


Fig. 6. Volume Acceleration vs. Excitation Current Calibration Curve of a Large Pentatondodecahedron Transducer.

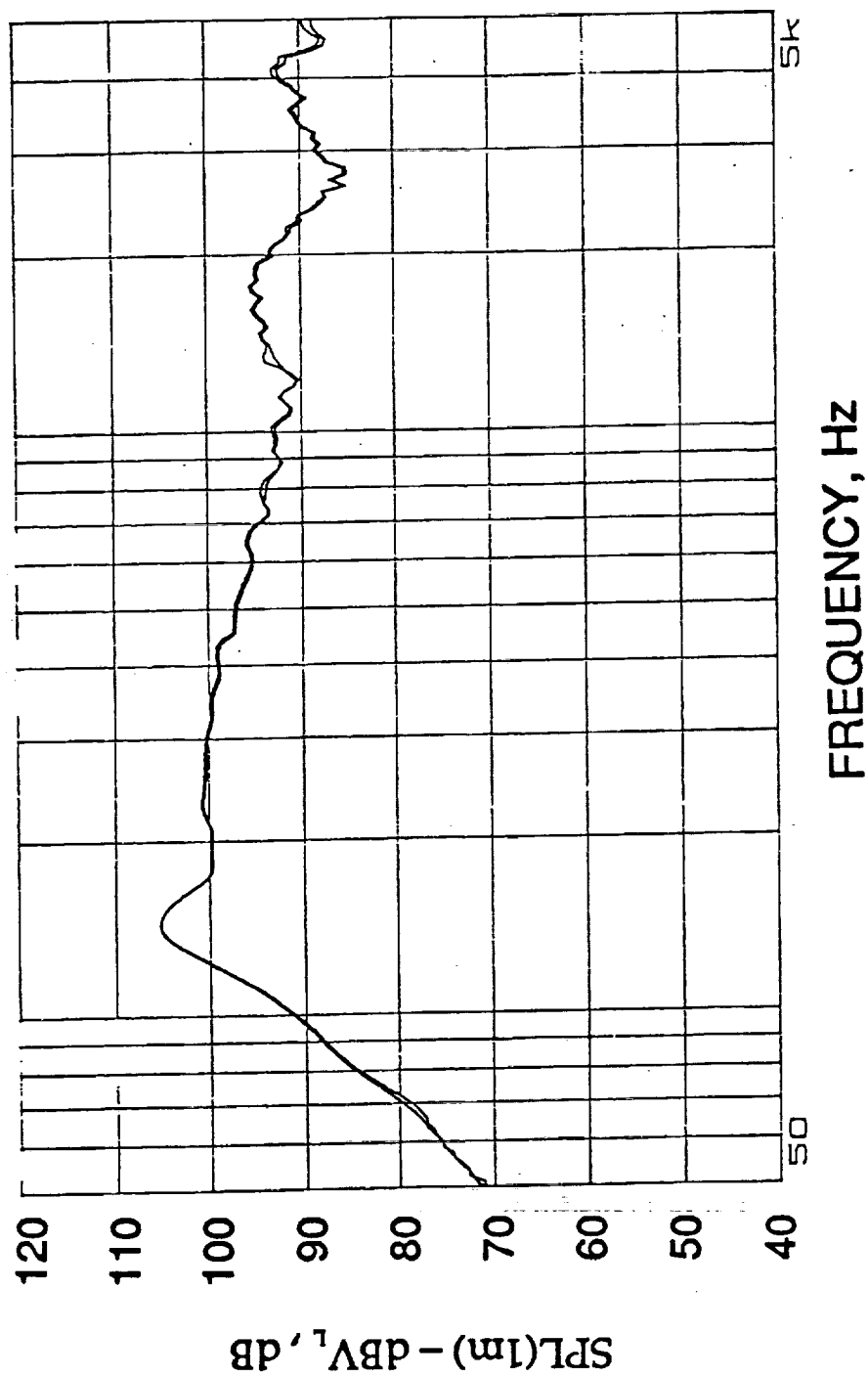
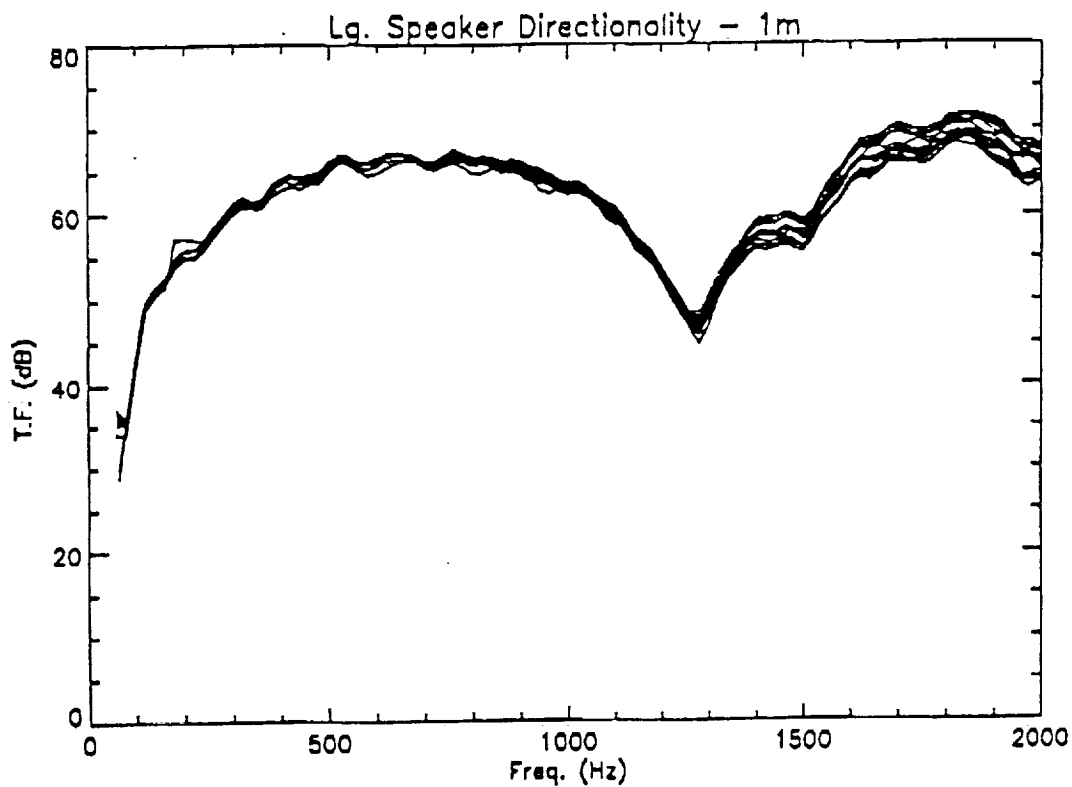
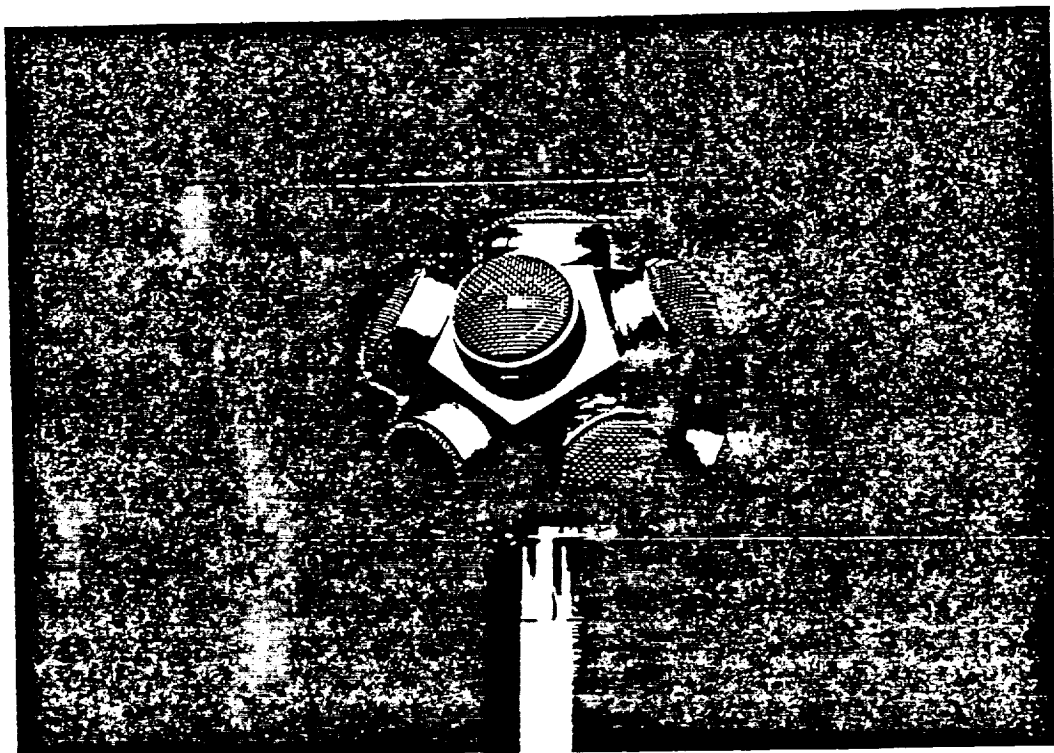


Fig. 7. Linearity Check; Sound Pressure Level at 1 Meter Minus Loudspeaker  
Excitation Voltage Level Obtained for 1 Volt and 10 Volt Loudspeaker  
Voltage.



**Fig. 8. Directionality Check; Transfer Function  
(Microphone Voltage/Loudspeaker Voltage)  
Measured at 10 Degree Incremental Rotation of the  
Large Transducer.**



**Fig. 9. Photograph of the Small Pentatondodecahedron Transducer.**

The wiring diagram of the small transducer is identical with that of the large transducer depicted in Fig. 3. The only difference is that the coil resistance of each tweeter is 4 Ohm, yielding a total resistance of 5.33 Ohm.

Figure 10 shows the transfer function between microphone voltage and the excitation voltage of the small transducer obtained by NASA at 1 meter microphone distance. The superimposed transfer functions were obtained by rotating the small transducer in 10 degree increments. The data in Fig. 10 indicate that the small transducer does not have an omni-directional radiation pattern. Since the large transducer covers the frequency range of interest from 100 Hz to 5 kHz, which is wider than anticipated, no attempts were made to investigate the reasons for the less than desirable directional characteristics of the small transducer.

### 3. RECIPROCITY EXPERIMENTS

Reciprocity experiments with two simultaneously acting forces and moment excitation were carried out by the NASA Langley research center on a 5.5 ft diameter, 12 ft long stiffened cylinder fuselage model. This section contains a brief description of the test article and the test results.

#### 3.1 Test Article

The reciprocity experiments were carried out by NASA Langley personnel utilizing an existing fuselage model made of carbon fibers embedded in epoxy resin. The fuselage model has the following characteristics.

Length:	3.6m (12 ft)
Diameter:	1.68m (5.5 ft)
Skin Thickness:	$1.7 \times 10^{-3}$ m (0.067 in)
Skin Young's Modulus:	$0.13 \times 10^{12}$ Pa for longitudinal direction $0.11 \times 10^{11}$ Pa for circumferential direction
Skin Shear Modulus:	$0.6 \times 10^{10}$ Pa
Skin Poisson Ratio:	0.3
Skin Density:	$1550 \text{ kg/m}^3$
Ring Frames:	10 J-section
Stringers:	22 hat-section, evenly spaced
Ends:	3 layers of 1.25 in. thick particle board



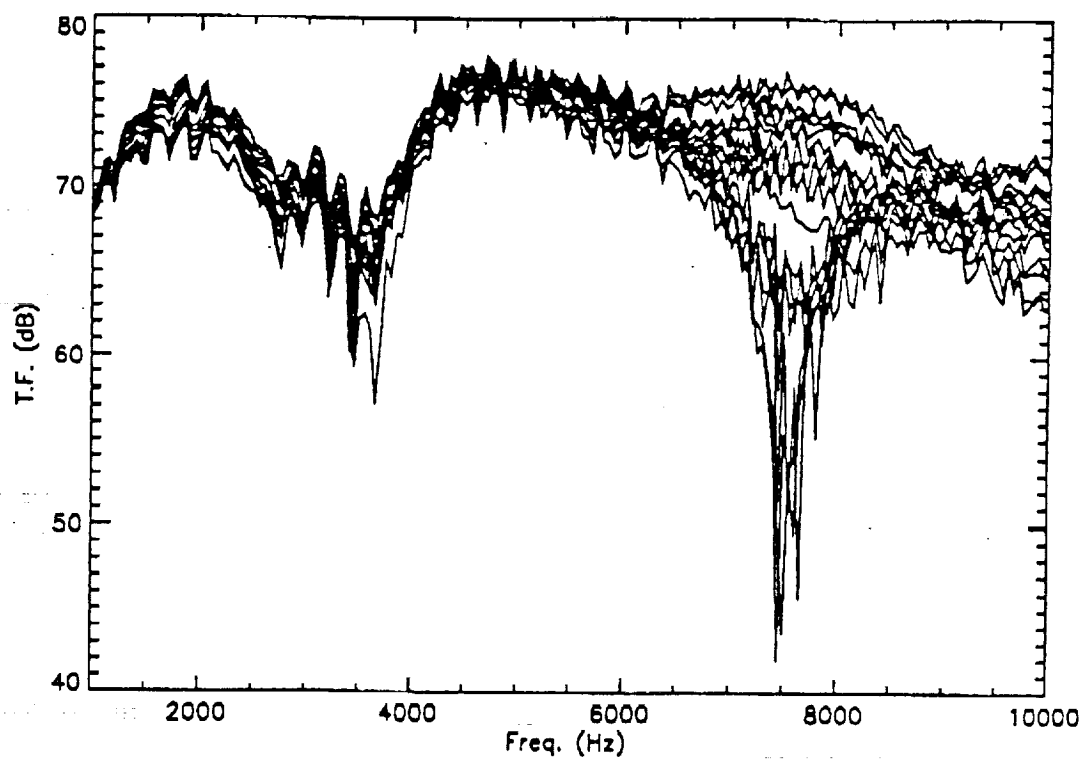


Fig. 10. Directivity Check; Transfer Function (Microphone Voltage/Loudspeaker Voltage) Measured at 10 Degree Incremental Rotation of the Small Transducer.

The mode shapes and resonance frequencies of the test article have been previously investigated and the results reported [4]. The first structural resonance occurs at 64 Hz and the first acoustic resonance of the interior volume at 47 Hz. To provide some acoustic damping a number of foam anechoic wedges were placed at the far end of the interior volume.

### 3.1 Two Force Excitation

In this experiment two coherent forces were applied to the test fixture by two shakers mounted 4 in. apart from each other. For the direct experiments each of the forces  $F_1$  and  $F_2$  were applied individually, then both forces were applied simultaneously. The acoustic response was recorded at four interior positions by measuring the open circuit voltage of the large reciprocity transducer placed at these four receiver positions A, B, C and D. Excitation and receiver positions are identified in Fig 11.

For the reciprocal experiments the large reciprocity transducer was working in its transmitting mode and for each position A, B, C and D the sound-induced vibration velocity response was measured by miniature accelerometers placed at the former two force excitation positions.

For the direct and the corresponding reciprocal experiments the following transfer functions were recorded.

No.	<u>Direct Transfer Function</u>	<u>Corresponding Reciprocal Transfer Function</u>
1	$U_{A1}/F_1$	$v_{1A}/i_A$
2	$U_{B1}/F_1$	$v_{1B}/i_B$
3	$U_{C1}/F_1$	$v_{1C}/i_C$
4	$U_{D1}/F_1$	$v_{1D}/i_D$
5	$U_{A2}/F_2$	$v_{2A}/i_A$
6	$U_{B2}/F_2$	$v_{2B}/i_B$
7	$U_{C2}/F_2$	$v_{2C}/i_C$
8	$U_{D2}/F_2$	$v_{2D}/i_D$
9	$U_A/(F_1+F_2)$	
10	$U_B/(F_1+F_2)$	
11	$U_C/(F_1+F_2)$	
12	$U_D/(F_1+F_2)$	

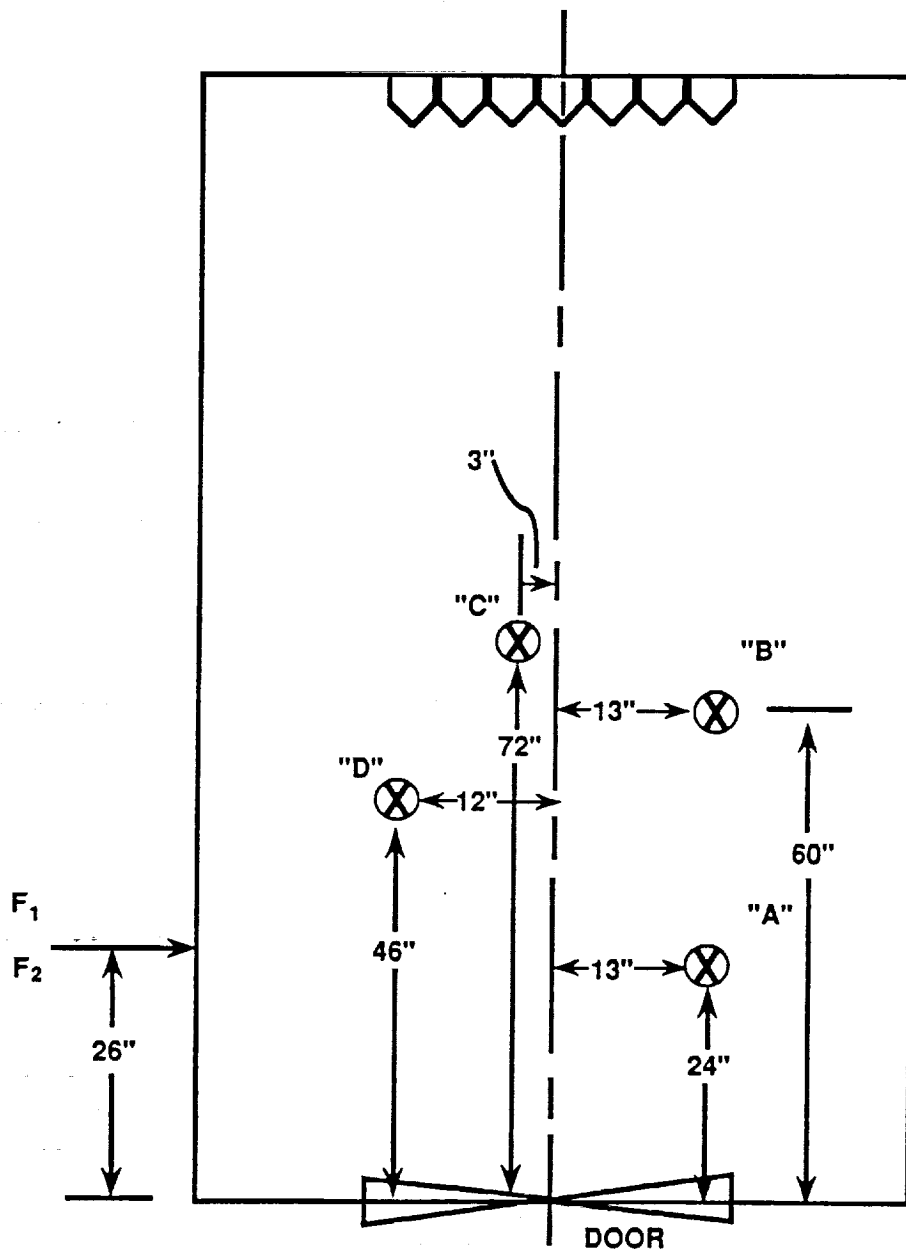


Fig. 11. Sketch of the Fuselage Model Identifying Excitation Positions 1 and 2 and Receiver Positions A, B, C and D.

The transfer function pairs 1 through 8 are shown in Figs. 12 through 19. Observing Figs. 12 through 15, (which display the direct and reciprocal transfer functions between Force Excitation Point 1 and the four Transducer Locations A, B, C and D) note that the reciprocal transfer functions  $v_i/i$  agree reasonably well with the directly measured transfer functions  $U/F_1$ . However, the transfer functions obtained for Force Excitation Point 2, as displayed in Figs. 16 through 19, yield less satisfactory agreement.

Figure 20A shows the input accelerance (acceleration/Force) measured at Pos. 1, and Fig. 20B the force spectrum measured at the same location. Figure 20C depicts the open circuit voltage response of the large transducer at Pos. C in response to the above force excitation at Pos. 1. The accelerance peaks at 316 Hz indicating a local resonance of the test fixture at this frequency. Below 316 Hz the structural response is stiffness controlled and above 316 Hz by the structural damping. The force spectrum at Pos. 1 peaks around 180 Hz and has a sharp minimum at 316 Hz where the first structural resonance occurs. The open circuit voltage peaks around 150 Hz where the transducer has its resonance frequency and the excitation force spectrum has a broad peak. The large fluctuations of the open circuit voltage response are due to acoustic resonances of the interior volume of the fixture and to standing wave patterns.

Figure 21 illustrates the extent of reproducibility of the excitation force measurements. After five successive reattachments of the shaker/force gauge assembly at Excitation Position 1, the transfer function  $TF_{1i} = F_{1i}/U_{1i}$  between the measured force  $F_{1i}$  and the applied shaker voltage  $U_{1i}$  was measured. The first transfer function  $TF_{10} = F_{10}/U_{10}$  was chosen as a reference to obtain the four normalized transfer functions  $TF_{11}/TF_{10}$ ,  $TF_{12}/TF_{10}$ ,  $TF_{13}/TF_{10}$  and  $TF_{14}/TF_{10}$ .

Nominally all of these normalized force spectra should be identical. The differences seen in Fig. 21 are due to slight changes caused by successive reattachment of the shaker/force gauge assembly. The spectral differences in Fig. 21 therefore represent the maximum achievable collapse between directly measured and reciprocally obtained transfer functions and, correspondingly, it is representative for the expected accuracy to predict Force F, from reciprocity measurements.

Figure 22 shows the ratio of the directly measured transfer function  $U_{C1}/F_{1C}$  and the reciprocally predicted transfer function  $v_{1C}/i_{C1}$ . Curve A represents the ratio of the magnitudes and Curve B the difference in phase. Differences are the largest where either one or both of the coherence functions, shown in Fig. 23, has a low value.

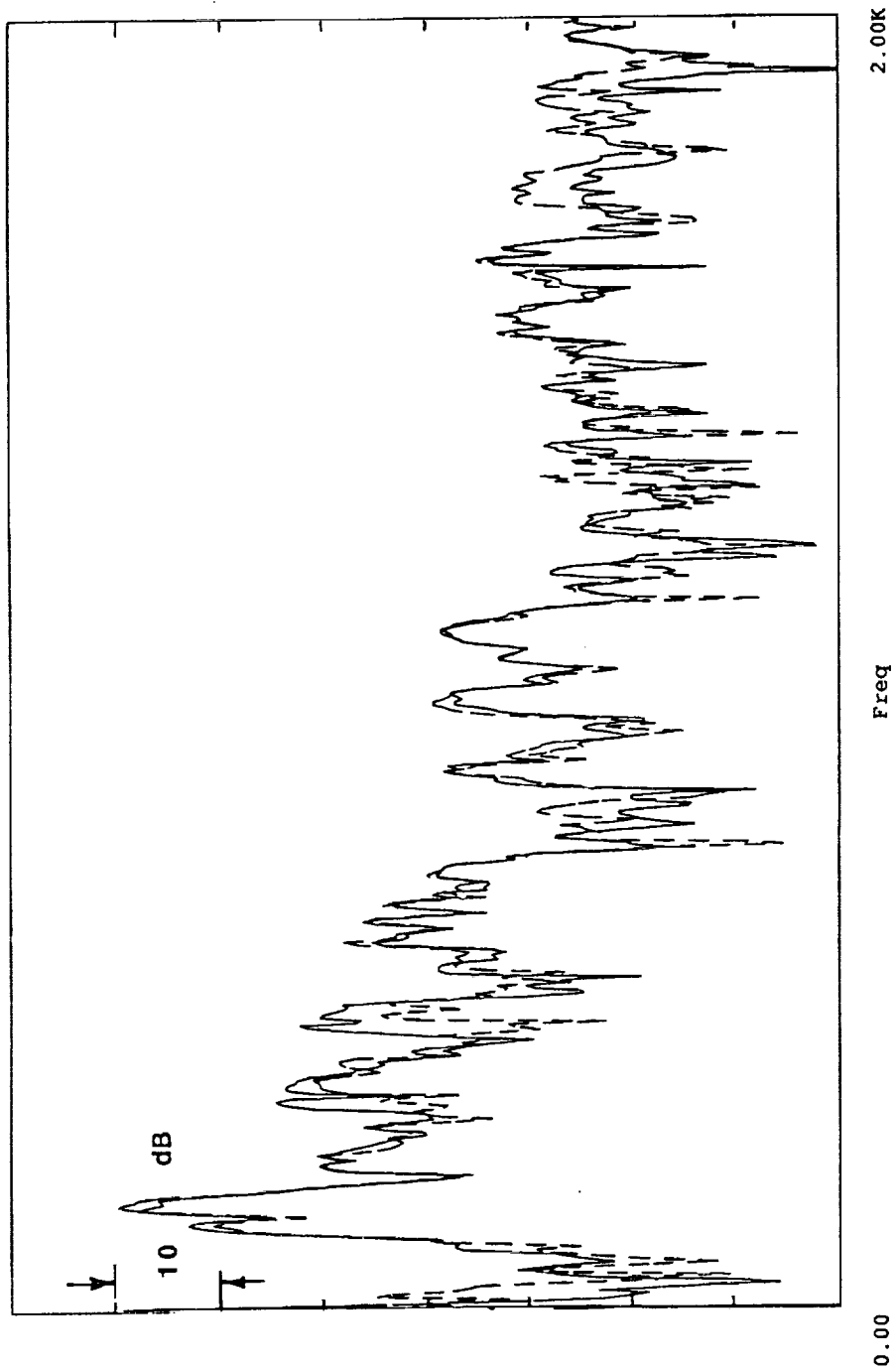


Fig. 12. Direct Transfer Function  $v_{A1}/F_1$  and  
Corresponding Reciprocal Transfer Function  
 $U_{1A}/i_A$ .

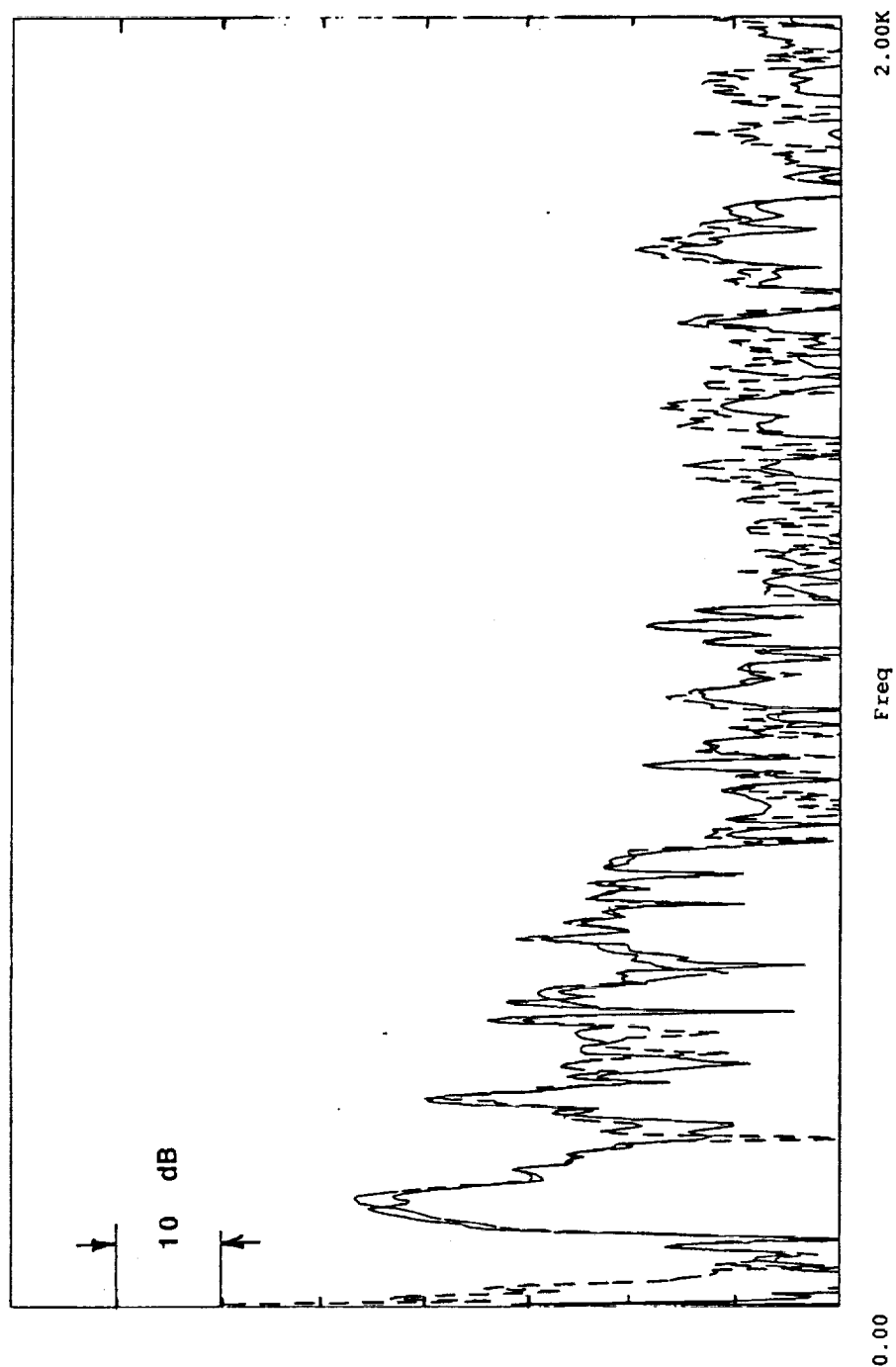


Fig. 13. Direct Transfer Function  $U_{B1}/F_1$  and  
Corresponding Reciprocal Transfer Function  
 $v_{1B}/i_B$ .

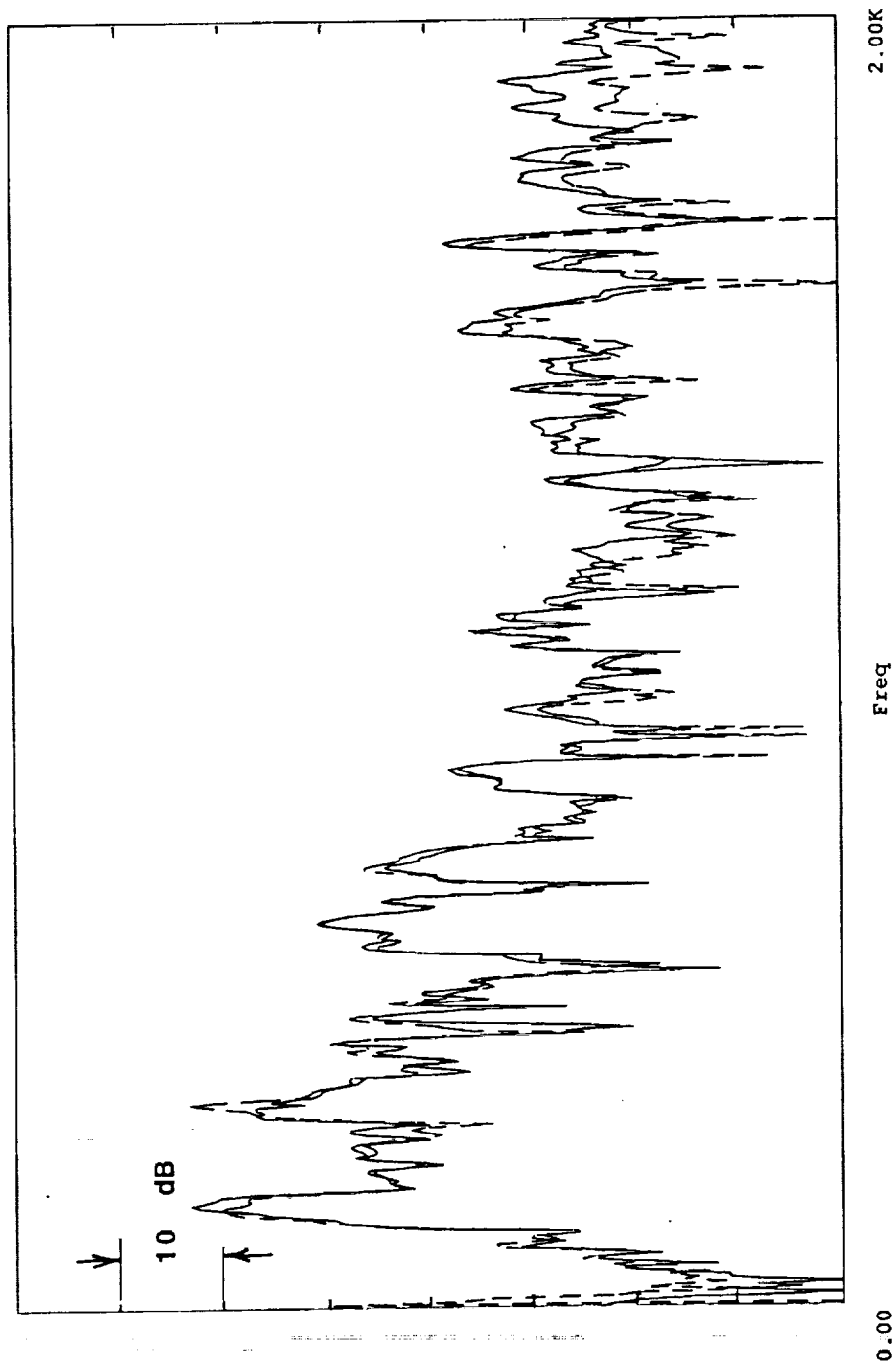


Fig. 14. Direct Transfer Function  $UC_1/F_1$  and  
Corresponding Reciprocal Transfer Function  
 $v_{1C}/i_C$ .



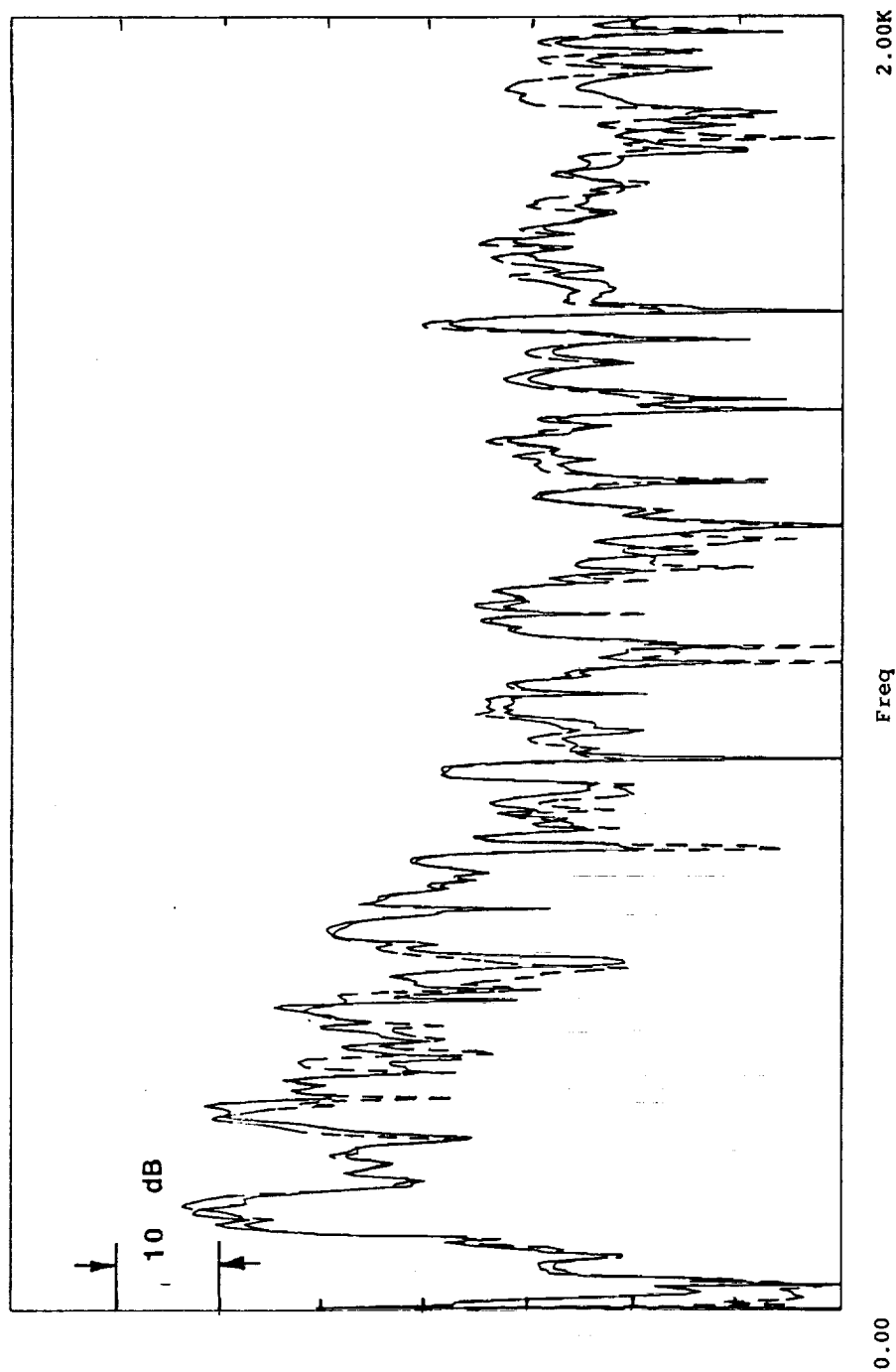


Fig. 15. Direct Transfer Function  $U_{D1}/F_1$  and  
Corresponding Reciprocal Transfer Function  
 $v_{1D}/i_D$ .

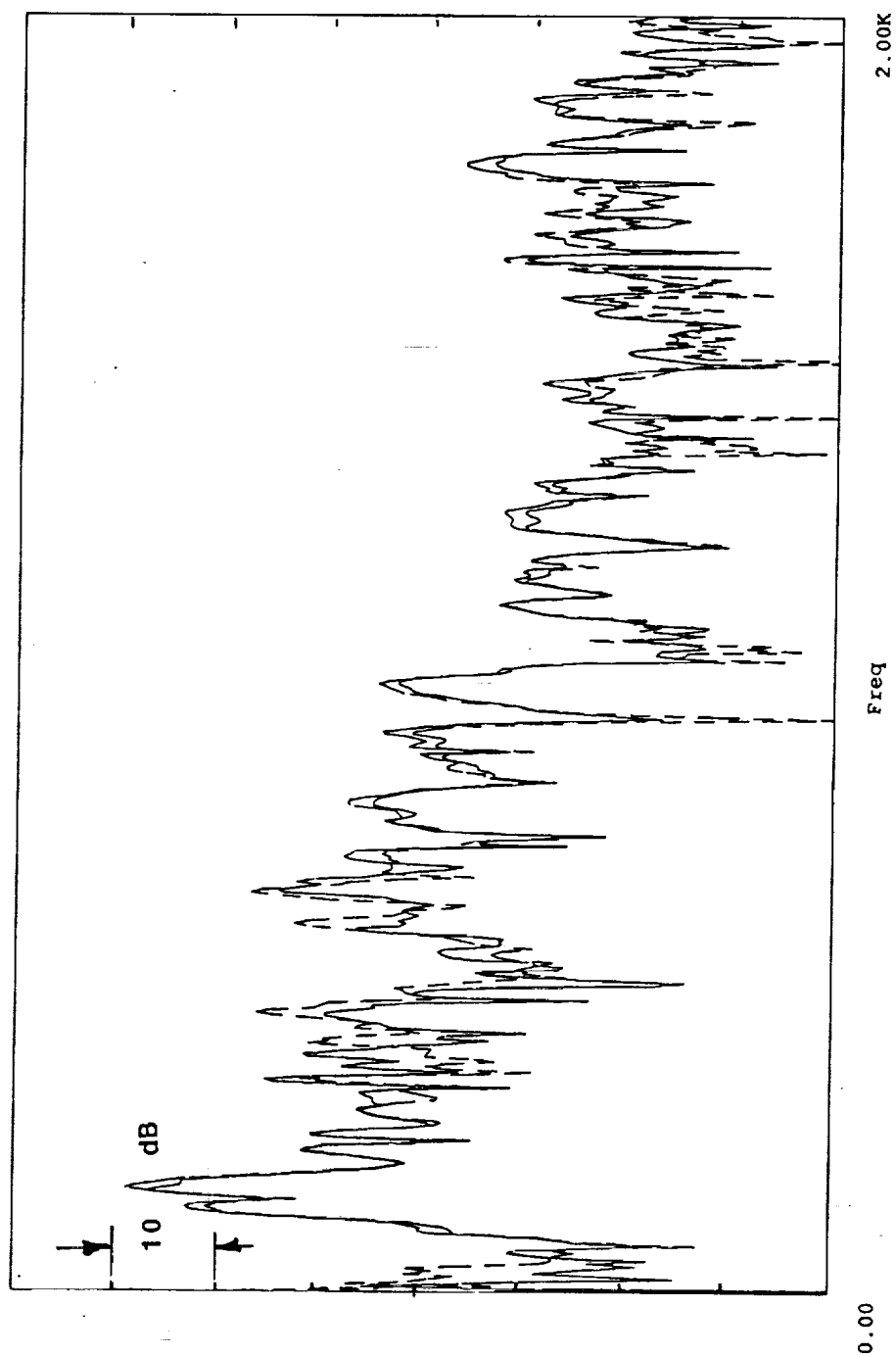


Fig. 16. Direct Transfer Function  $U_{A2}/F_2$  and  
Corresponding Reciprocal Transfer Function  
 $v_{2A}/i_A$ .

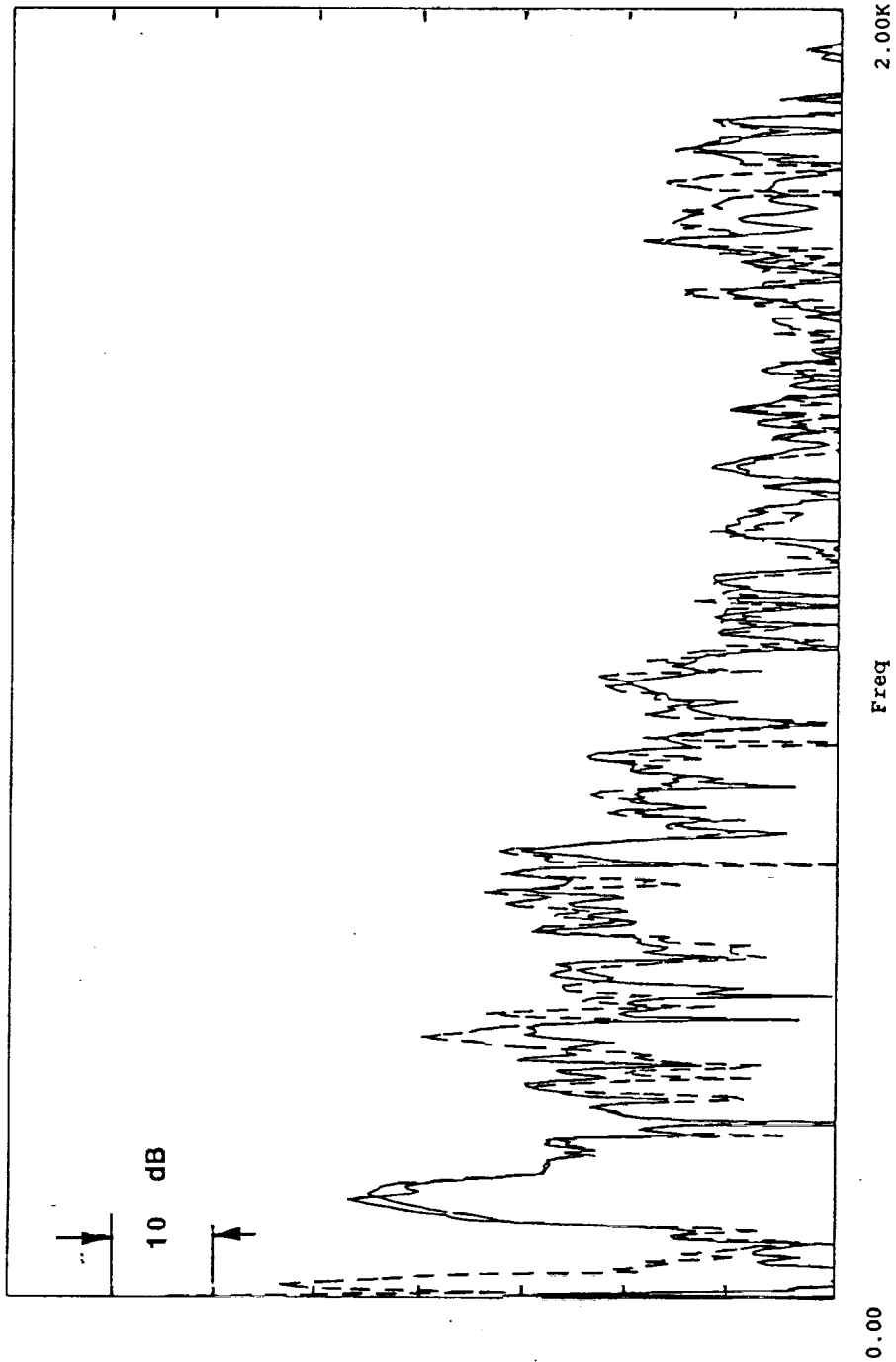


Fig. 17. Direct Transfer Function  $U_{B2}/F_2$  and  
Corresponding Reciprocal Transfer Function  
 $v_{2B}/i_B$ .

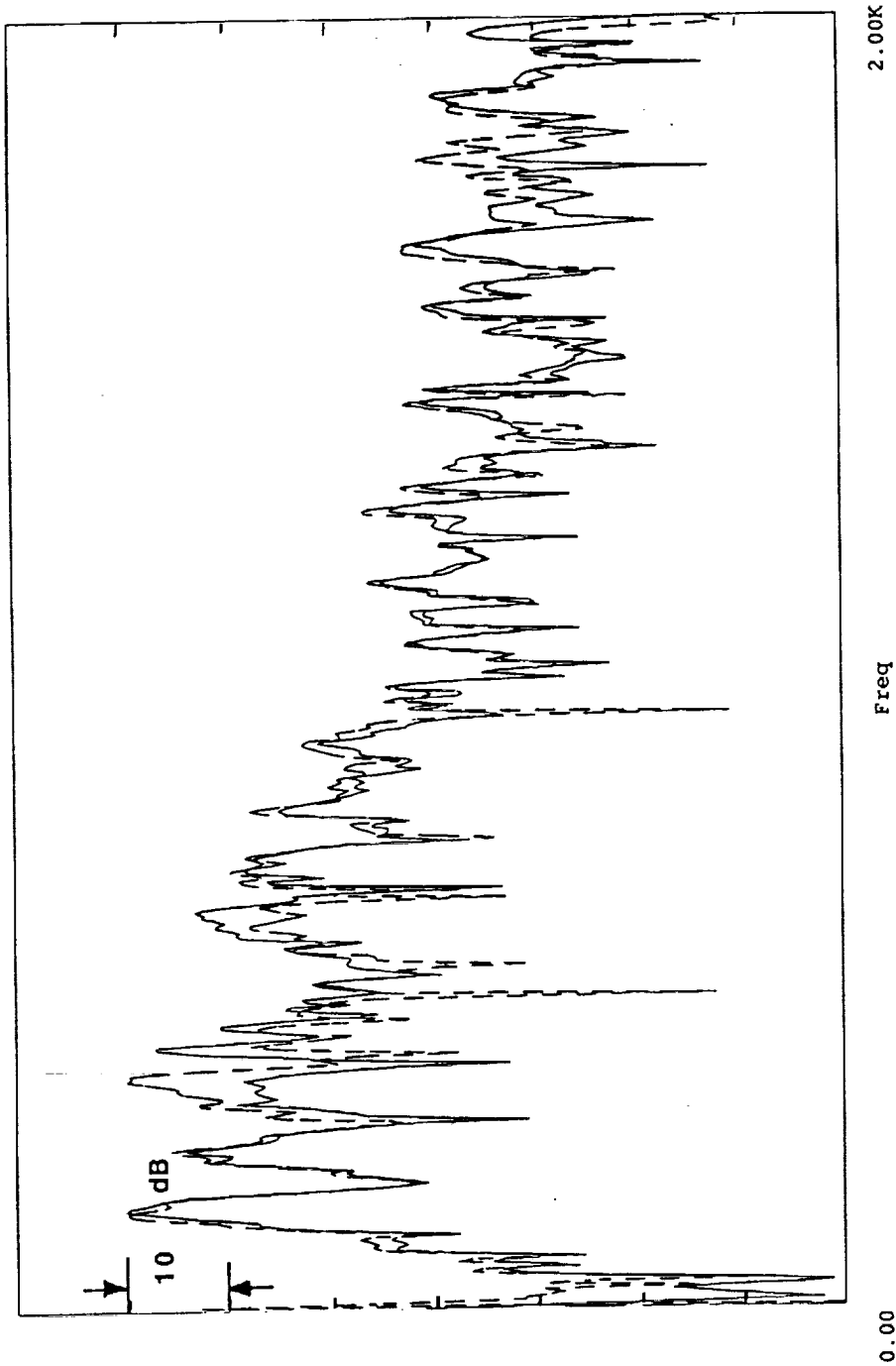


Fig. 18. Direct Transfer Function  $U_{C2}/F_2$  and  
Corresponding Reciprocal Transfer Function  
 $v_{2C}/i_C$ .

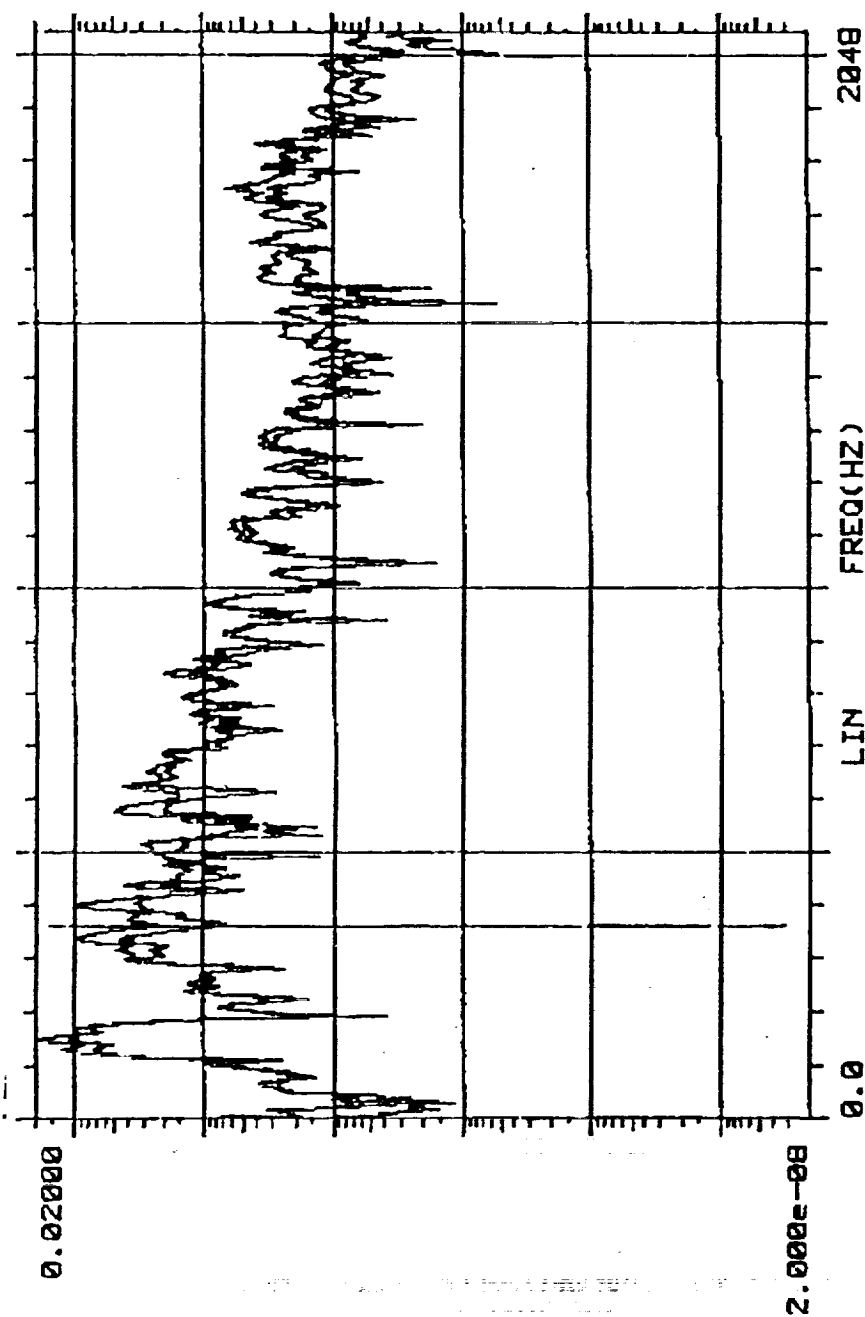


Fig. 19. Direct Transfer Function  $U_{D2}/F_2$  and  
Corresponding Reciprocal Transfer Function  
 $v_{2D}/i_D$ .

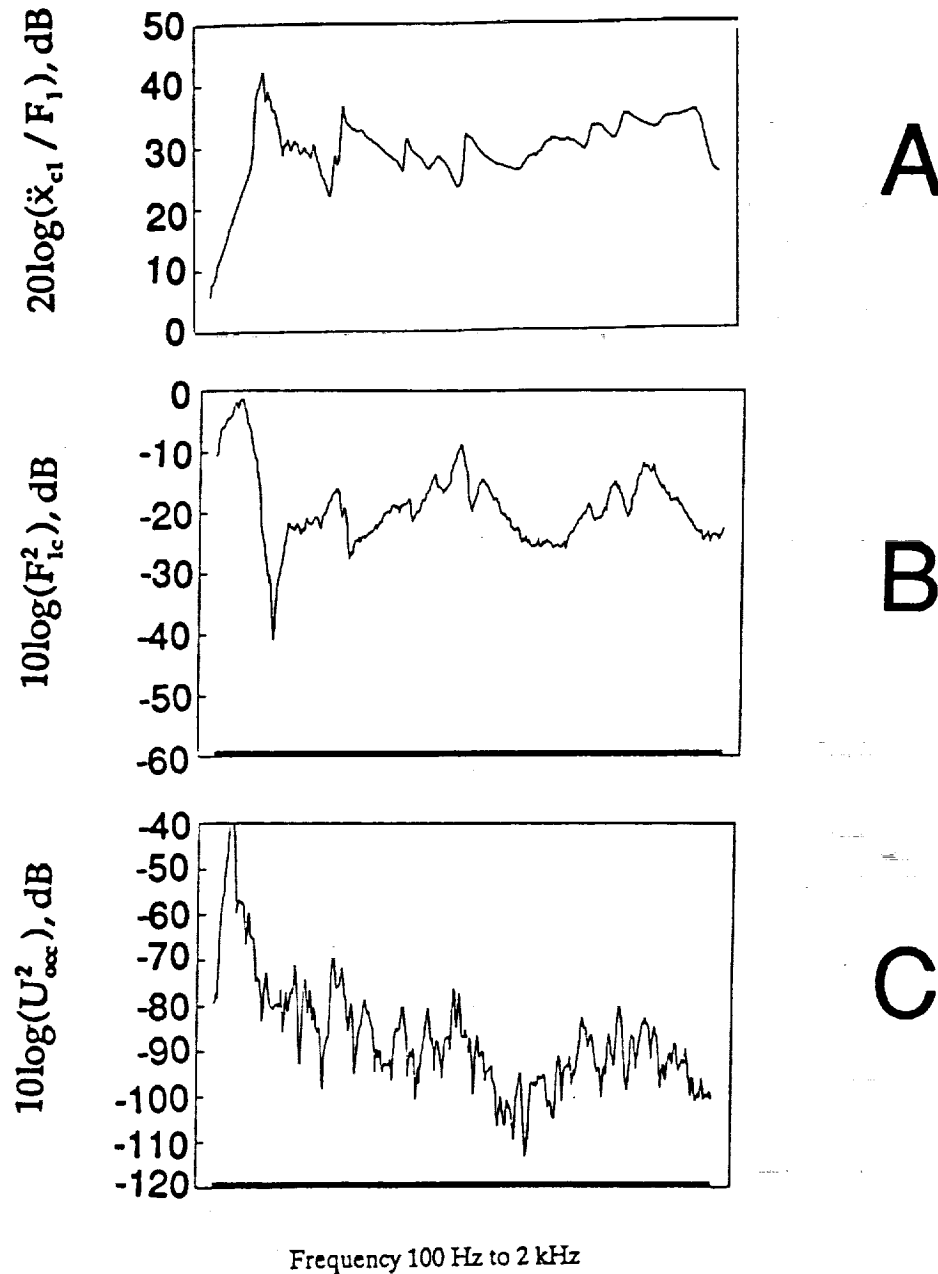
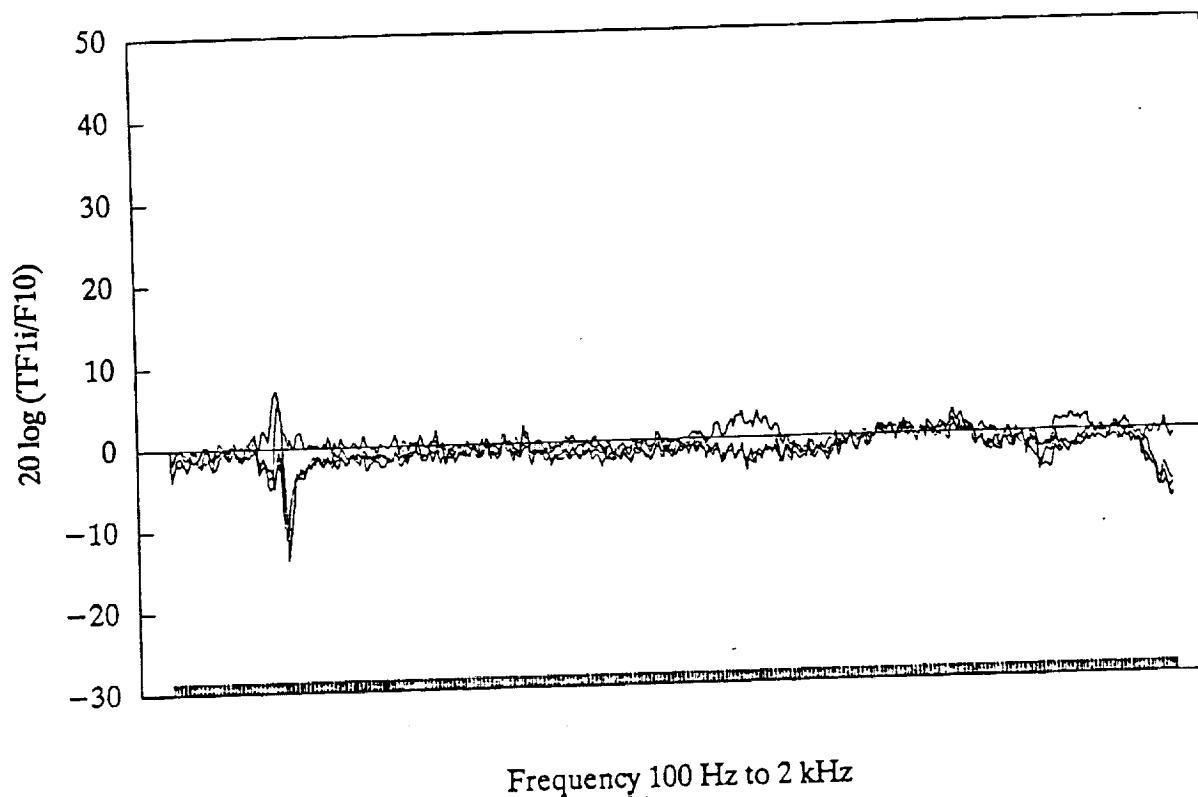


Fig. 20. Driving Point Input and Response Characteristics, Excitation Pos. 1 Transducer Location C.

A. Input Accelerance at Pos. 1

B. Force Spectrum at Pos. 1

C. Open circuit voltage Response at Pos. C



**Fig. 21** Change In Excitation Force/Shaker Voltage Transfer Function Due To Five Successive Reattachments Of The Shaker/Force Gauge Assembly At Excitation Position 1

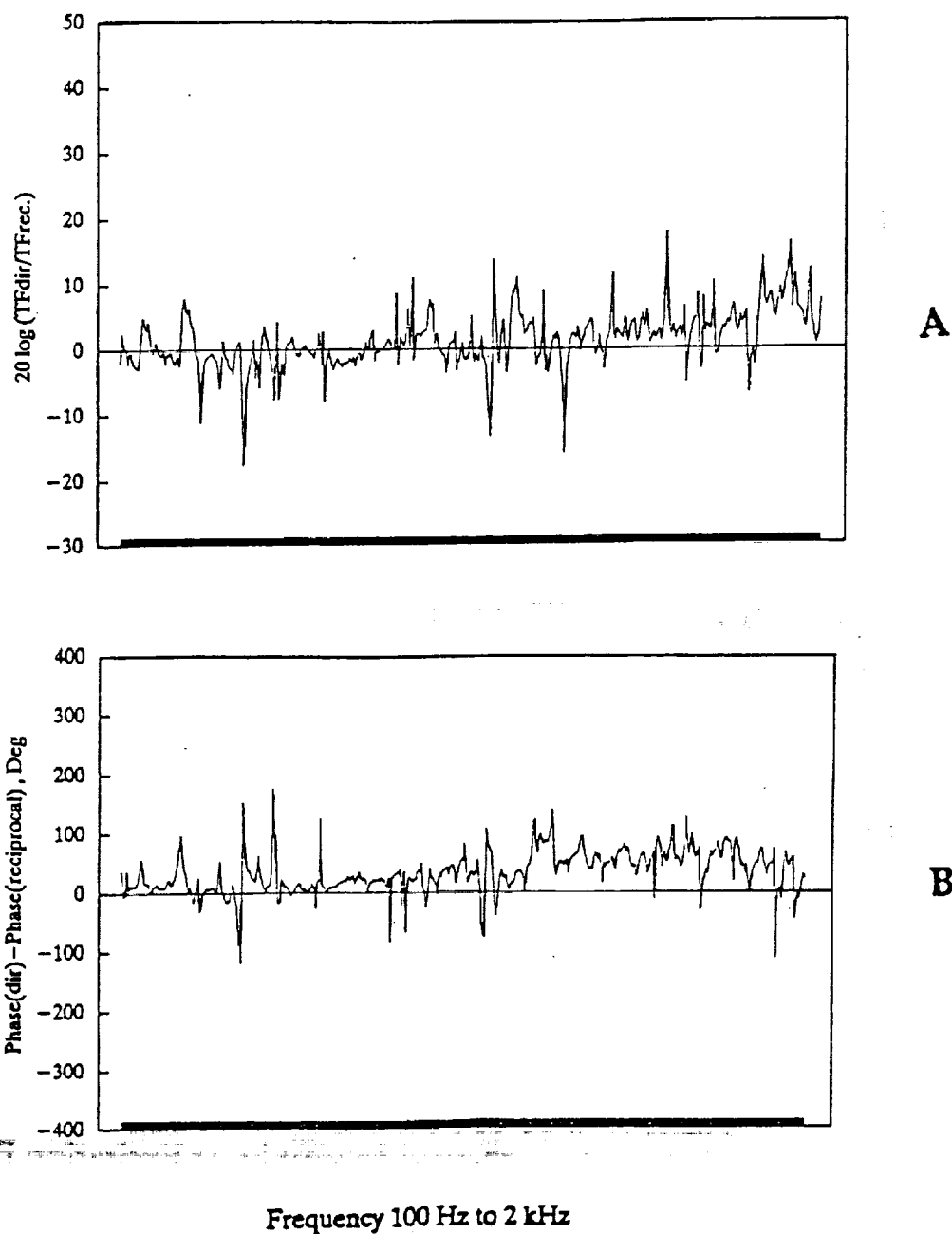
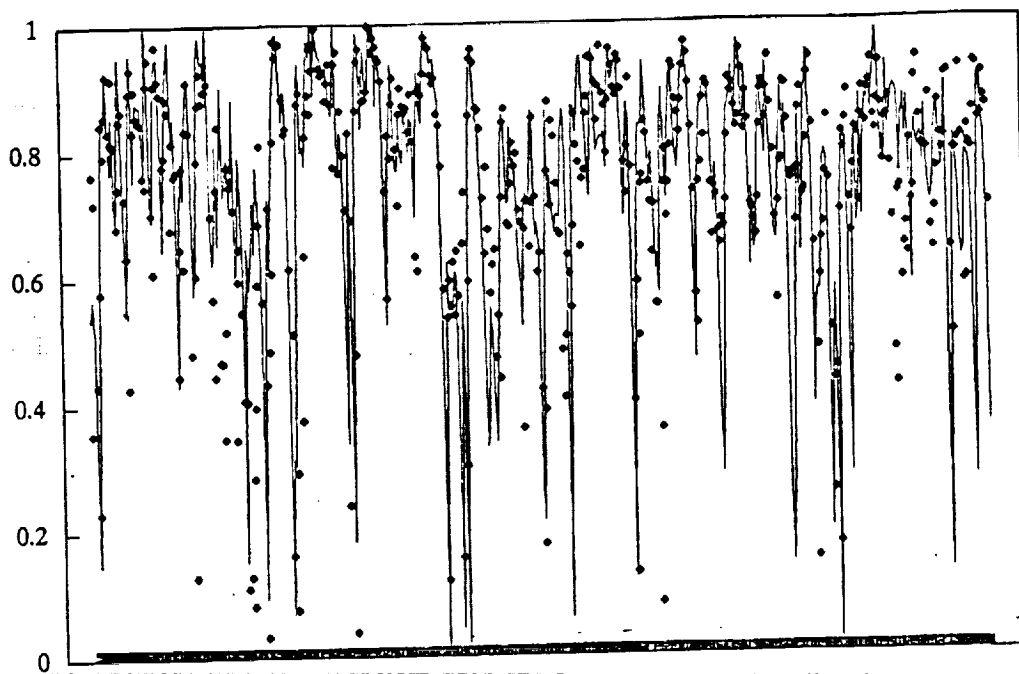


Fig. 22. Comparison of the Directly Measured Transfer Function  $U_{C1}/F_{1C}$  with Reciprocity Prediction  $v_{1C}/i_{C1}$

A. Magnitude ratio

B. Phase difference





Frequency 100 Hz to 2 kHz

— Reciprocal    • Direct

Fig. 23. Coherence Functions

— direct,  $U_{C1}/F_{1C}$

◆ reciprocal,  $v_{1C}/i_{C1}$

Figure 24 shows how averaging can improve the reciprocity prediction of excitation force  $F_1$ . The top curve shows the ratio of the four individual direct vs. reciprocal transfer functions measured for transducer locations A, B, C and D. A further frequency averaging (e.g. in 1/3-octave bands) would result in even smaller differences.

Figure 25 shows the driving point accelerance (acceleration/force) at Pos. 2. It is substantially different from the driving point accelerance at Pos. 1 depicted in Figure 20.

Figure 26 shows the change in force spectra at excitation Pos. 2 due to successive reattachments of the shaker/force gauge assembly. When compared with Fig. 21, obtained for excitation Pos. 1, note that the repeatability at Pos. 2 is not as good as was in Pos. 1.

Figure 27 shows the results of predicting force  $F_2$  from the reciprocal transfer functions. The top graph shows each of the four individual predictions while the middle graph shows the average of these four predictions. Just as was the case at Pos. 1, (see Fig. 24) the averaging here also improves the prediction accuracy. As shown in the bottom graph, a frequency averaging in 1/3-octave bands yields further improvements in prediction accuracy.

The error in measuring excitation force is larger than the random error (exemplified by the less than desirable repeatability) because it also entails systematic errors caused by the fact that the impedance of the shaker mounting hardware (located between the force sensor and the test object) is not negligibly small compared with the point impedance of the test object, especially at resonance frequencies of the structure where the input impedance takes very low values. Consequently, further refinement of our ability to measure the excitation force accurately should be achieved before a reciprocity analyses is attempted to predict the magnitude and phase of two coherent excitation forces  $F_1$  and  $F_2$  when they act simultaneously.

### 3.2 Moment Excitation

The moment excitation to the test fixture was applied by attaching a rigid 1.75 in. long beam stub perpendicular to its skin and applying a force in a direction perpendicular to both the cylinder axis and to the beam stub. This way the cantilevered beam stub exerted a combination of a moment and an in-plane force on the test fixture's skin. The direct transfer functions were defined as the  $U/F_0$  where  $U$  is the open circuit voltage of the reciprocity transducer and  $F_0$  is the force applied to the beam. The corresponding reciprocal transfer function was  $v_0/i$  where  $v_0$  is the velocity response at the former force excitation location and  $i$  is the current driving the reciprocity transducer. Figure 28 shows one of the representative pairs of transfer functions. The agreement between the transfer function pairs is unsatisfactory. It is believed that the lack of agreement results from the fact that in measuring the reciprocal transfer function, the predominant motion of the skin of the test fixture is radial and the cross sensitivity of the accelerometer is not sufficiently low to enable it to measure the much smaller circumferential motion of the beam end caused by the rotational motion of the skin.

It is believed that improvements in measurement techniques and signal processing procedures can be found which will enable us to perform reciprocity prediction of exiting moments with sufficient accuracy for engineering use.

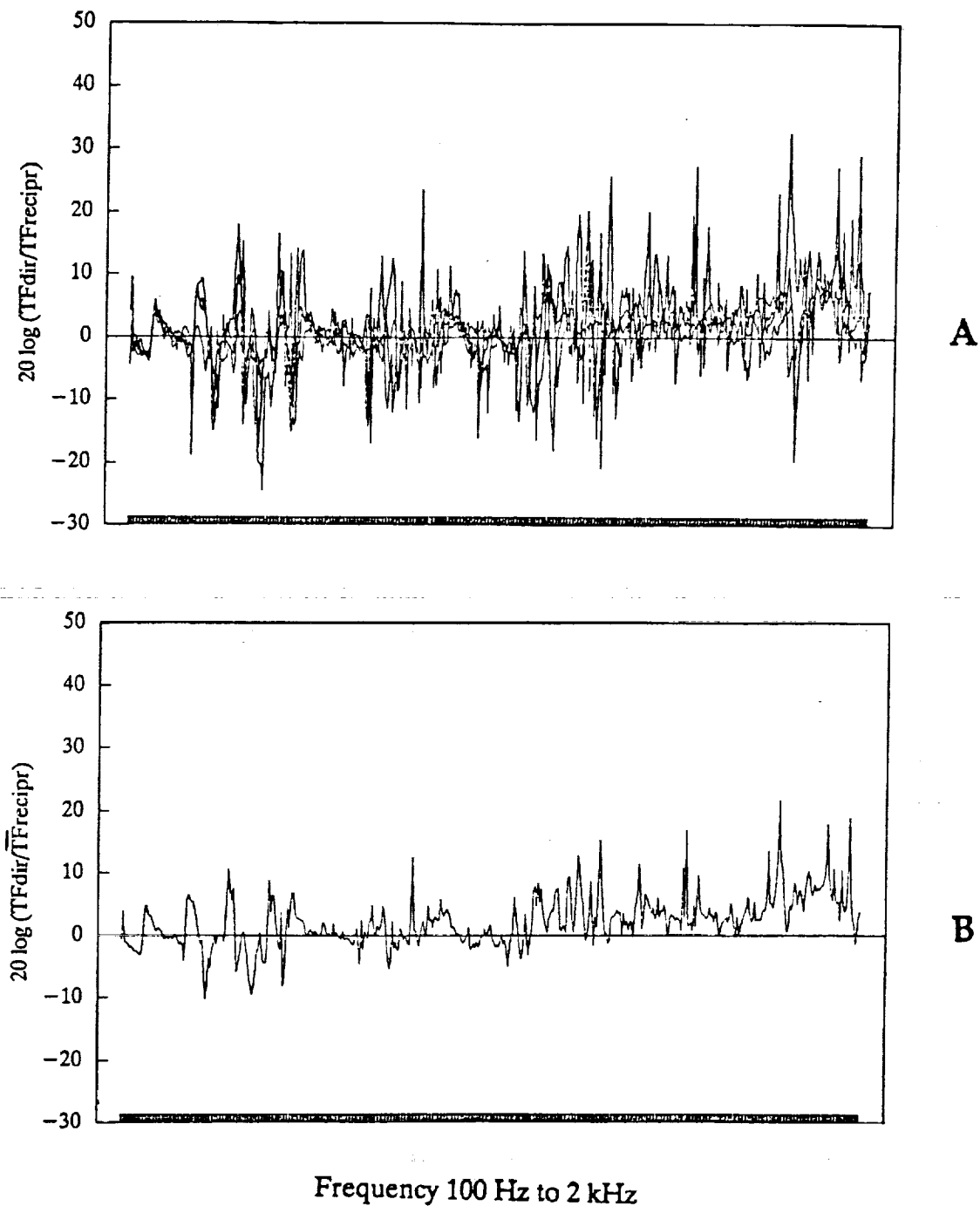


**Fig. 24. Effect of Averaging on Reciprocity Prediction;**  
**Force Excitation at Pos. 1; Transducer Locations A,**  
**B, C and D**

**A. Ratio of individual transfer functions**

**B. Ratio of averaged transfer functions**

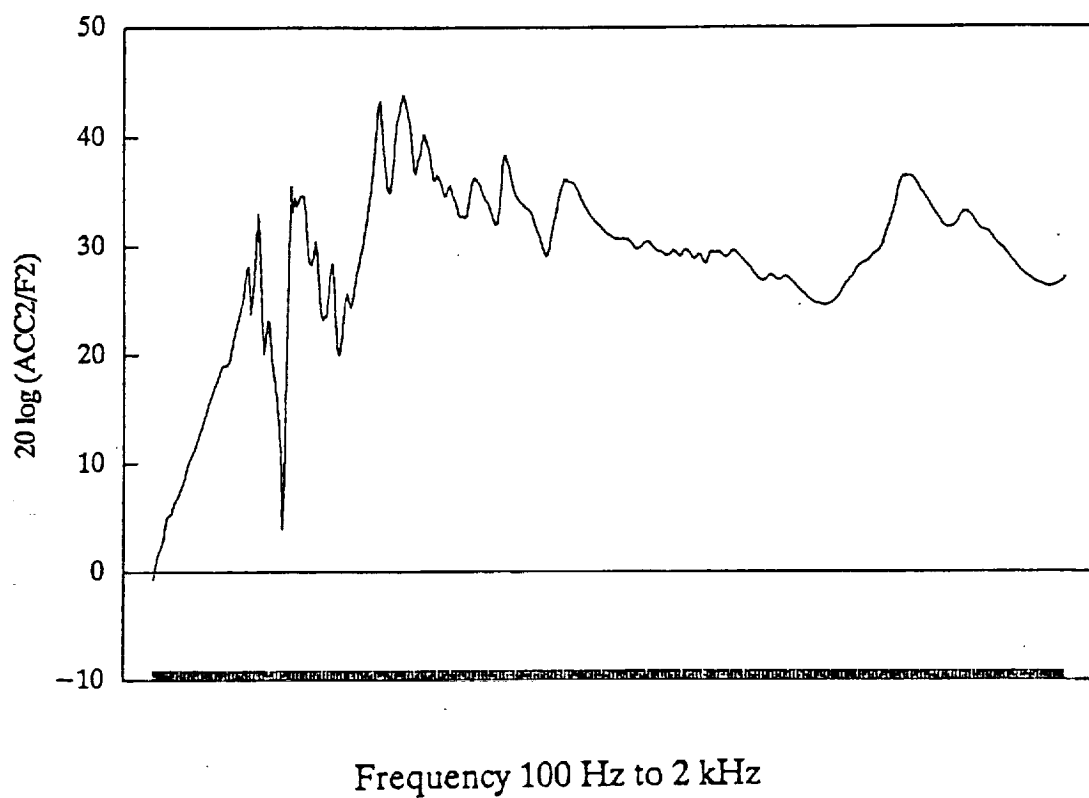


Fig. 25. Input Accelerance at Excitation Point 2.

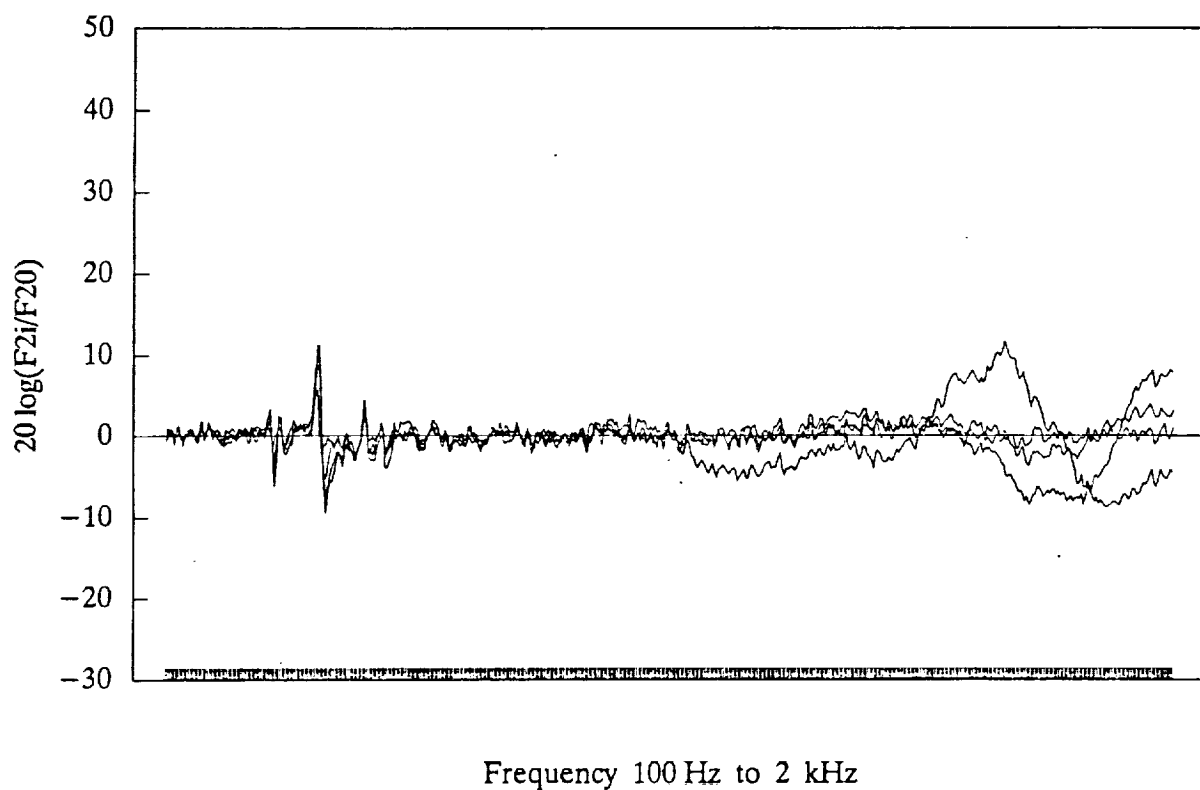


Fig. 26. Change in Force Spectra due to Successive Reattachments of the Shaker/Force Gauge Assembly at Excitation Point 2.

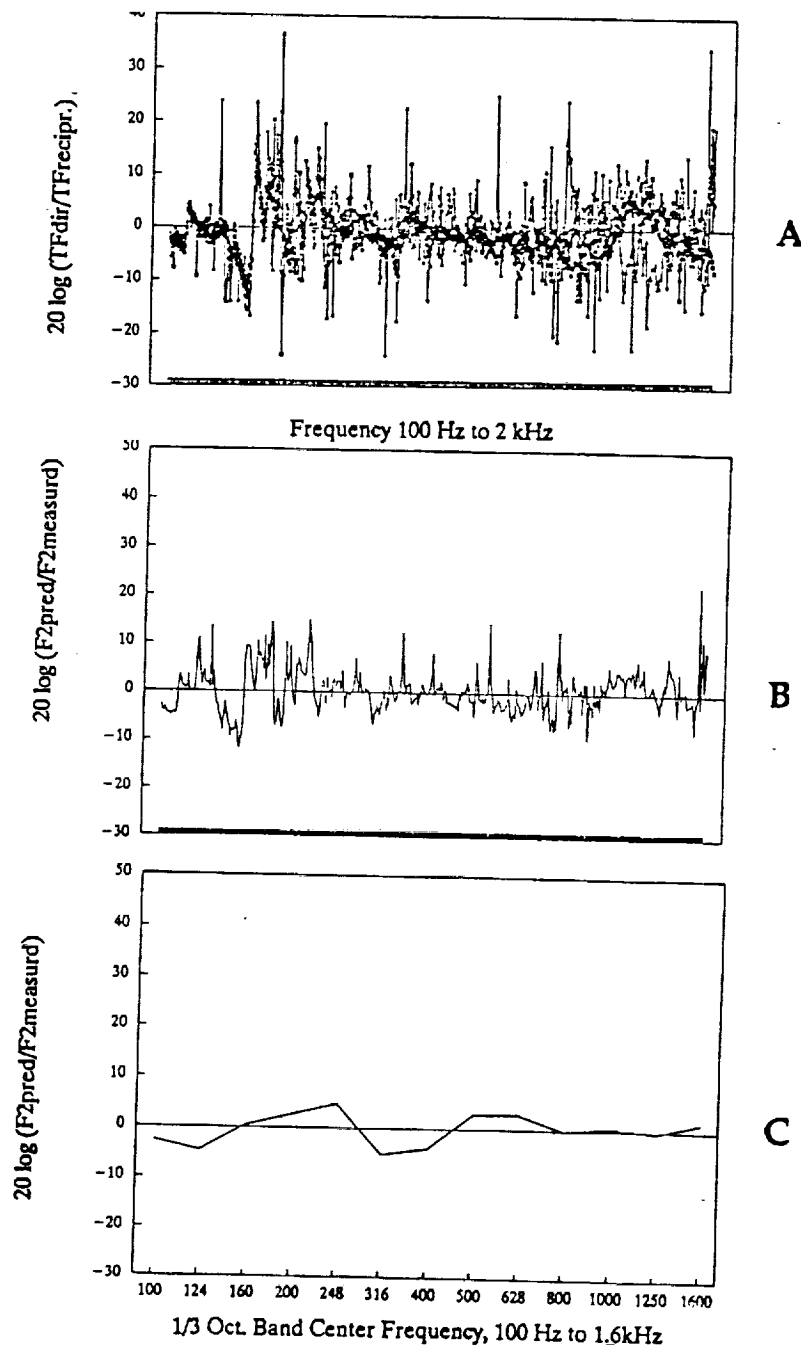


Fig. 27. Prediction of Force  $\bar{F}_2$  Utilizing Reciprocity

- A. Individual prediction from transducer locations A, B, C and D
- B. Average of the four predictions
- C. Curve B, frequency averaged in 1/3-octave bands

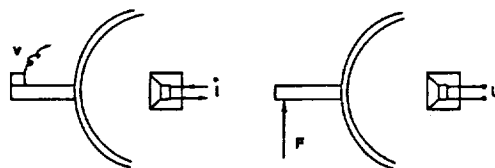
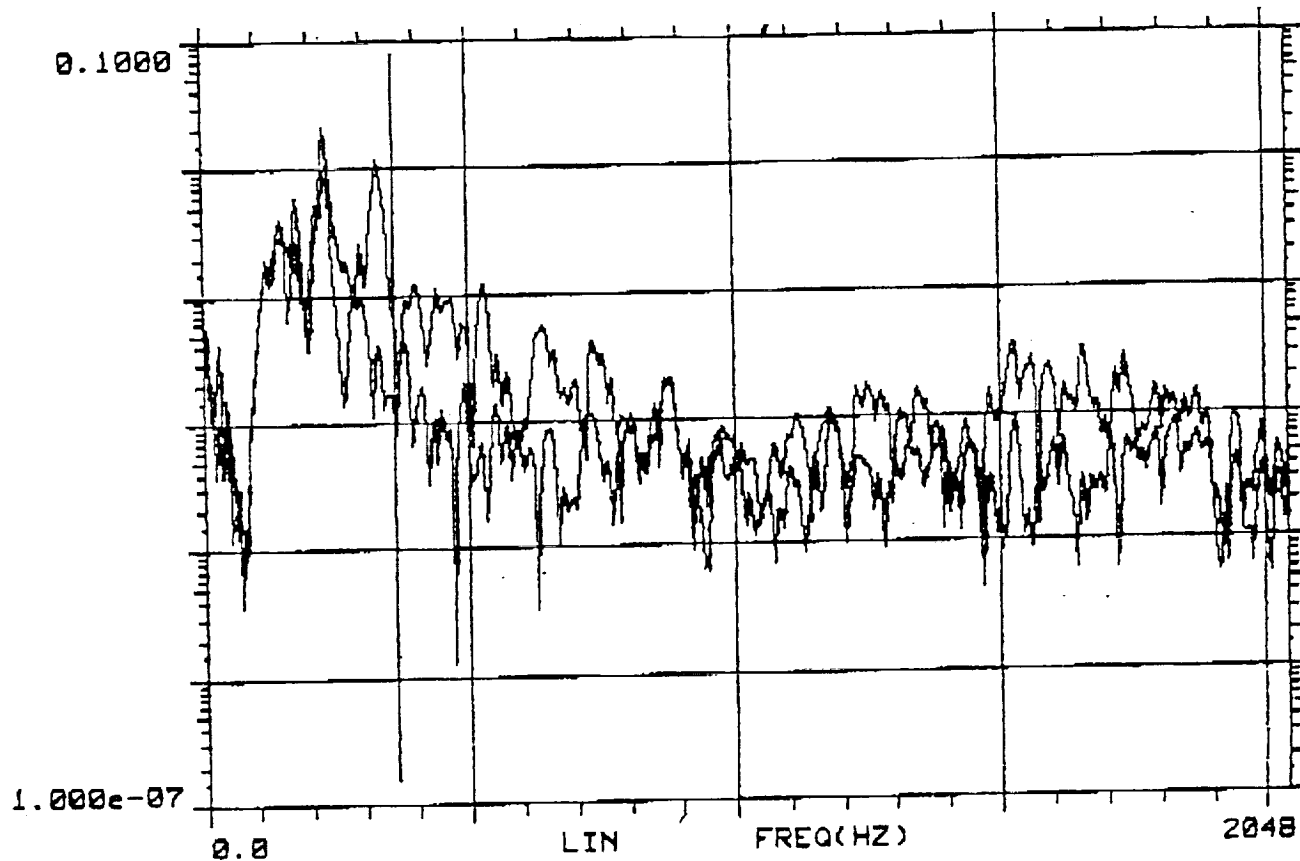


Fig. 28. Comparison of the Direct and Reciprocal Transfer Function Obtained for Moment Excitation.



## REFERENCES

1. Vér, I.L. "Reciprocity as a Prediction and Diagnostic Tool in Reducing Transmission of Structureborne and Airborne Noise into an Aircraft Fuselage; Volume 1: Proof of Feasibility", BBN Report 4985 (July 1982), NASA Contract No. NAS1-16521, Task Order Number 11.
2. Vér, I.L. "Reciprocity as a Prediction and Diagnostic Tool in Reducing Transmission of Structureborne and Airborne Noise into an Aircraft Fuselage; Volume 2: Feasibility of Predicting Interior Noise due to Multiple, Correlated Force Inputs", BBN Report 6259 (May 1986), NASA Contract No. NAS1-16521, Task Order Number 18.
3. Vér, I.L. "Reciprocity and Superposition" Section 9.9, Noise and Vibration Control Engineering, L.L. Beranek and I.L. Vér Edts., John Wiley and Sons, New York 1992, pp 317-328.
4. Grosveld, F.W. and T.F. Beyer "Modal Characteristics of a Stiffened Composite Cylinder with Open and Closed End Conditions" AIAA-86-1909.



## APPENDIX A

### Sensitivity Analysis of the Redundancy on Prediction Accuracy



### §1 Formulation of an analytical scheme

**The Reciprocal Theorem** Consider a mechanical system of elastic structures immersed in a stationary acoustic medium, as indicated schematically in Figure 1. Forces  $F_1, F_2, \dots$ , are applied at the points labeled respectively 1, 2, ..., in the figure. These forces produce velocities  $V_1, V_2, V_3, \dots$ , at points labeled  $\bar{1}, \bar{2}, \bar{3}, \dots$ .

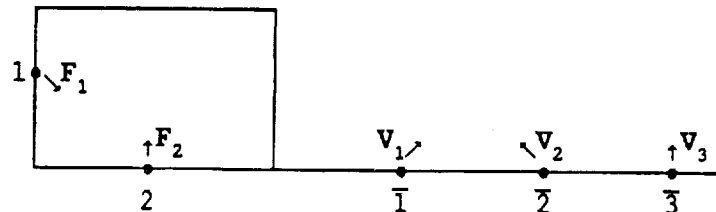


Figure 1 The direct problem

Consider next a reciprocal problem in which forces  $f_1, f_2, f_3, \dots$ , are applied at  $\bar{1}, \bar{2}, \bar{3}, \dots$ , producing velocities  $v_1, v_2, \dots$ , at points 1, 2, ... (Figure 2).

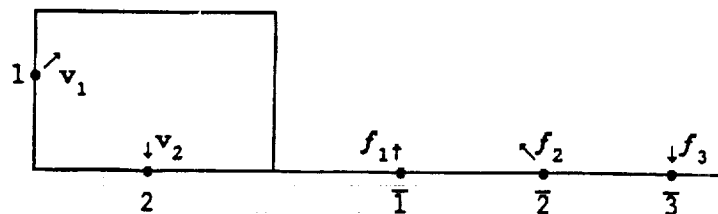


Figure 2 The reciprocal problem

According to the Reciprocal Theorem [1],

$$F_1 \cdot v_1 + F_2 \cdot v_2 + \dots = f_1 \cdot v_1 + f_2 \cdot v_2 + f_3 \cdot v_3 + \dots \quad (1)$$

The theorem remains valid if one or more of the forces are replaced by couples, in the following sense. Let a couple  $M_3$  be applied at point 3 in the direct problem, and let the reciprocal forces  $f_1, f_2, f_3, \dots$ , produce an angular velocity  $\omega_3$  at point 3 in the structure, then equation (1) becomes,

$$F_1 \cdot v_1 + F_2 \cdot v_2 + M_3 \cdot \omega_3 \dots = f_1 \cdot v_1 + f_2 \cdot v_2 + f_3 \cdot v_3 + \dots \quad (2)$$

To take account of all possibilities we shall adopt a notation in which,  $F_1, F_2, M_3$ , etc, are denoted by the *generalized forces*  $P_1, P_2, P_3$ , etc, and the corresponding velocities and angular velocities  $v_1, v_2, \omega_3$ , etc, are replaced by *generalized velocities*  $q_1, q_2, q_3$ , etc. The reciprocal theorem may then be expressed in the composite form,

$$\sum_{i=1}^N P_i \cdot q_i = \sum_{i=1}^M f_i \cdot v_i \quad (3)$$

where  $N$  and  $M$  are arbitrary.

**Application to source strength evaluation** Equation (3) forms the basis for the experimental determination of unknown forces  $P_i$  arising in a "direct" experiment in terms of observed values of the velocities  $V_i$  and of the velocities  $q_i$  when auxiliary, reciprocal experiments are performed with known forces  $f_i$ . It is assumed that experimental data are available for the velocities  $V_i$  from observations of the direct experiment, and that we are at liberty to choose the forces  $f_i$  in the reciprocal experiments in an arbitrary manner. In each of these latter experiments all of the  $f_i$  are zero except one component of one of the forces, making a total of  $3M$  experiments in which the velocities  $q_i$  are to be measured.

To simplify the description of the analysis we introduce the notation:

1. The forces  $P_i$ ,  $i = 1, 2, 3, \dots, N$ , are represented by the  $3N$ -dimensional vector  $P_i$ ,  $i = 1, 2, 3, \dots, 3N$ . This means that  $P_1 = (P_1, P_2, P_3)$ ,  $P_2 = (P_4, P_5, P_6)$ , etc.

2. The velocities  $V_i$ ,  $i = 1, 2, 3, \dots, M$ , are represented by the  $3M$ -dimensional vector  $V_i$ ,  $i = 1, 2, 3, \dots, 3M$ , so that  $V_1 = (V_1, V_2, V_3)$ ,  $V_2 = (V_4, V_5, V_6)$ , etc. .
3. In the  $3M$  reciprocal experiments the forces  $f_i$  are defined by  $f_1 = (f_1, f_2, f_3)$ ,  $f_2 = (f_4, f_5, f_6)$ , etc., where in the first reciprocal experiment  $f_1$  is the only non-zero component of force, in the second only  $f_2$  is non-zero, etc.
4. In the  $j$ th reciprocal experiment the generalized velocities  $q_i$ ,  $i = 1, 2, 3, \dots, N$ , are denoted by the  $3N$ -dimensional vector  $q_{ji}$  ( $i = 1$  to  $3N$ ), where  $q_1 = (q_{j1}, q_{j2}, q_{j3})$ ,  $q_2 = (q_{j4}, q_{j5}, q_{j6})$ , etc.

For each of the  $3M$  reciprocal experiments the reciprocal theorem can be applied in the form,

$$\sum_{i=1}^{3N} q_{ji} P_i = f_j V_j, \quad j = 1, 2, 3, \dots, 3M. \quad (4)$$

The quantity  $q_{ji}$  is a matrix of order  $3M \times 3N$  (i.e.,  $3M$  rows and  $3N$  columns). To calculate the unknown forces  $P_i$  from this system of equations the number of reciprocal experiments  $3M$  must be at least as large as  $3N$ . In practice, however, the data relating to the direct and reciprocal velocities  $V_i$ ,  $q_{ji}$  will be contaminated by noise, and it will be advisable to use an *overdetermined* system of equations to improve the accuracy of the predictions. This means that  $M > N$ , and equations (4) must then be solved by the method of least squares [2], according to which the solution vector  $P_i$  of (4) is chosen to minimize the squared residual

$$r^2 = \sum_{j=1}^{3M} \left[ \sum_{i=1}^{3N} q_{ji} P_i - f_j V_j \right]^2. \quad (5)$$

Taking the derivative of this equation with respect to  $P_i$  and equating the result to zero, we obtain the following system of equations for the determination of the  $P_i$ :

$$\sum_{j=1}^{3M} \sum_{\ell=1}^{3N} q_{ji} q_{j\ell} P_\ell = \sum_{j=1}^{3M} q_{ji} f_j V_j, \quad i = 1, 2, 3, \dots, 3N. \quad (6)$$

These equations are called the *normal equations* of the system. Observe that

$\sum_{j=1}^{3M} q_{ji} q_{j\ell}$  is a square matrix of order  $3N \times 3N$ , and the system (6) is just sufficient to determine the unknown forces  $P_i$ ,  $i = 1, 2, 3, \dots, 3N$ , in terms of the overspecified data furnished by the  $3M$  reciprocal experiments. In the unlikely event that all the data have been obtained without error, the solution of (6) will be independent of the value of  $M$  when  $M > N$ .

## §2 Sensitivity analysis

It may be assumed that the amplitudes of the reciprocal force-velocity products  $f_j V_j$  are all normalized to unity. To simplify the notation we write [3],

$$\alpha_{ij} = \sum_{j=1}^{3M} q_{ki} q_{kj}, \quad y_i = f_i V_i, \quad (7)$$

and define the  $3N \times 3N$  matrix  $C_{ij}$  to be the inverse of  $\alpha_{ij}$ , i.e.,

$$\sum_{k=1}^{3N} C_{ik} \alpha_{kj} = \delta_{ij}. \quad (8)$$

Assume that the respective errors  $\epsilon_i, \epsilon_j$  in the force-velocity products  $y_i = f_i V_i, y_j = f_j V_j$  are uncorrelated for  $i \neq j$ , and that the mean square errors  $\epsilon^2$ , say, are equal, i.e.,

$$\langle \epsilon_i \epsilon_j \rangle = \epsilon^2 \delta_{ij}, \quad (9)$$

where the angle brackets  $\langle \rangle$  denote a time average. The corresponding error  $\delta P_i$  in  $P_i$  is given by,

$$\delta P_i = \sum_{j=1}^{3M} \epsilon_j \frac{\partial P_i}{\partial y_j}. \quad (10)$$

Hence,

$$\langle (\delta P_i)^2 \rangle = \sum_{j=1}^{3M} \sum_{k=1}^{3M} \langle \epsilon_j \epsilon_k \rangle \frac{\partial P_i}{\partial y_j} \frac{\partial P_i}{\partial y_k} = \sum_{j=1}^{3M} \epsilon^2 \left( \frac{\partial P_i}{\partial y_j} \right)^2. \quad (11)$$

To calculate  $\partial P_i / \partial y_j$  we use,

$$P_i = \sum_{k=1}^{3N} C_{ik} \sum_{j=1}^{3M} q_{jk} y_j, \quad (12)$$



so that,

$$\frac{\partial P_i}{\partial y_j} = \sum_{k=1}^{3N} C_{ik} q_{jk} \quad (13)$$

Thus,

$$\begin{aligned} \langle (\delta P_i)^2 \rangle &= \sum_{k=1}^{3N} \sum_{\ell=1}^{3N} C_{ik} C_{i\ell} \sum_{j=1}^{3M} \epsilon^2 q_{jk} q_{j\ell} \\ &= \epsilon^2 \sum_{k=1}^{3N} \sum_{\ell=1}^{3N} C_{ik} C_{i\ell} \alpha_{k\ell} \end{aligned} \quad (14)$$

Using equation (8), this finally yields,

$$\langle (\delta P_i)^2 \rangle = \epsilon^2 C_{ii} \quad (15)$$

**Example** Consider the case of two generalized forces  $P_1$ ,  $P_2$ , and write equations (4) in the form,

$$\begin{pmatrix} \lambda_1 & \mu_1 \\ \lambda_2 & \mu_2 \\ \lambda_3 & \mu_3 \\ \dots & \dots \\ \lambda_{3M} & \mu_{3M} \end{pmatrix} \begin{pmatrix} P_1 \\ P_2 \end{pmatrix} = \begin{pmatrix} y_1 \\ y_2 \\ y_3 \\ \dots \\ y_{3M} \end{pmatrix} \quad (16)$$

where  $\lambda = (q_{11}, q_{21}, \dots, q_{3M,1})$ ,  $\mu = (q_{12}, q_{22}, \dots, q_{3M,2})$ . In shorthand notation, (16) can be written,

$$\begin{pmatrix} \lambda & \mu \end{pmatrix} \begin{pmatrix} P_1 \\ P_2 \end{pmatrix} = \begin{pmatrix} y \end{pmatrix} \quad (17)$$

The transposed matrix  $\begin{pmatrix} \lambda & \mu \end{pmatrix}^T = \begin{pmatrix} \lambda \\ \mu \end{pmatrix}$ , and,

$$\alpha_{ij} = \begin{pmatrix} \lambda^2 & \lambda \cdot \mu \\ \lambda \cdot \mu & \mu^2 \end{pmatrix} \quad (18)$$

It follows that,

$$\left. \begin{aligned} P_1 &= \frac{\hat{\lambda} \cdot y - (\hat{\lambda} \cdot \hat{\mu})(\hat{\mu} \cdot y)}{|\lambda| [1 - (\hat{\lambda} \cdot \hat{\mu})^2]} \\ P_2 &= \frac{\hat{\mu} \cdot y - (\hat{\lambda} \cdot \hat{\mu})(\hat{\lambda} \cdot y)}{|\mu| [1 - (\hat{\lambda} \cdot \hat{\mu})^2]} \end{aligned} \right\} \quad (19)$$

where,

$$\hat{\lambda} = \lambda/|\lambda|, \quad \hat{\mu} = \mu/|\mu|. \quad (20)$$

The corresponding error estimates are,

$$\left. \begin{aligned} \langle (\delta P_1)^2 \rangle^{1/2} &= \frac{\epsilon}{|\lambda| \sqrt{1 - (\hat{\lambda} \cdot \hat{\mu})^2}} \\ \langle (\delta P_2)^2 \rangle^{1/2} &= \frac{\epsilon}{|\mu| \sqrt{1 - (\hat{\lambda} \cdot \hat{\mu})^2}} \end{aligned} \right\} \quad (21)$$

Provided  $\sqrt{1 - (\hat{\lambda} \cdot \hat{\mu})^2}$  remains bounded, equations (21) imply that the errors decrease like  $\epsilon/(3M)^{1/2}$  as  $M$  becomes large.

It can frequently happen that the normal equations (6) are ill-conditioned. The matrix  $\alpha_{ij}$  is then very nearly singular (in the two dimensional example above it corresponds to  $\sqrt{1 - (\hat{\lambda} \cdot \hat{\mu})^2}$  being nearly equal to zero). When this occurs the normal equations can be solved by the method of "singular value decomposition", which is described in detail in Reference 3.

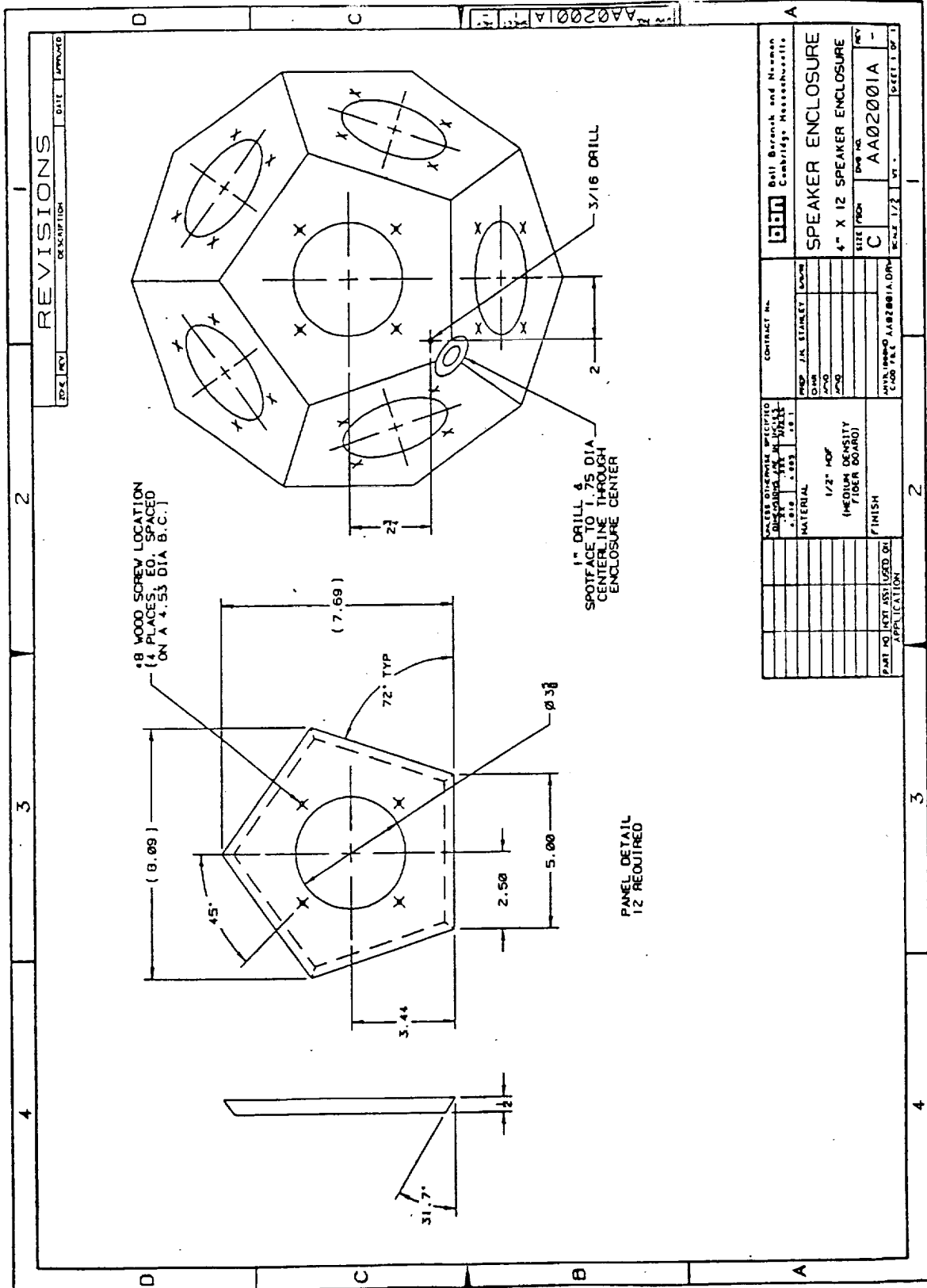
#### References

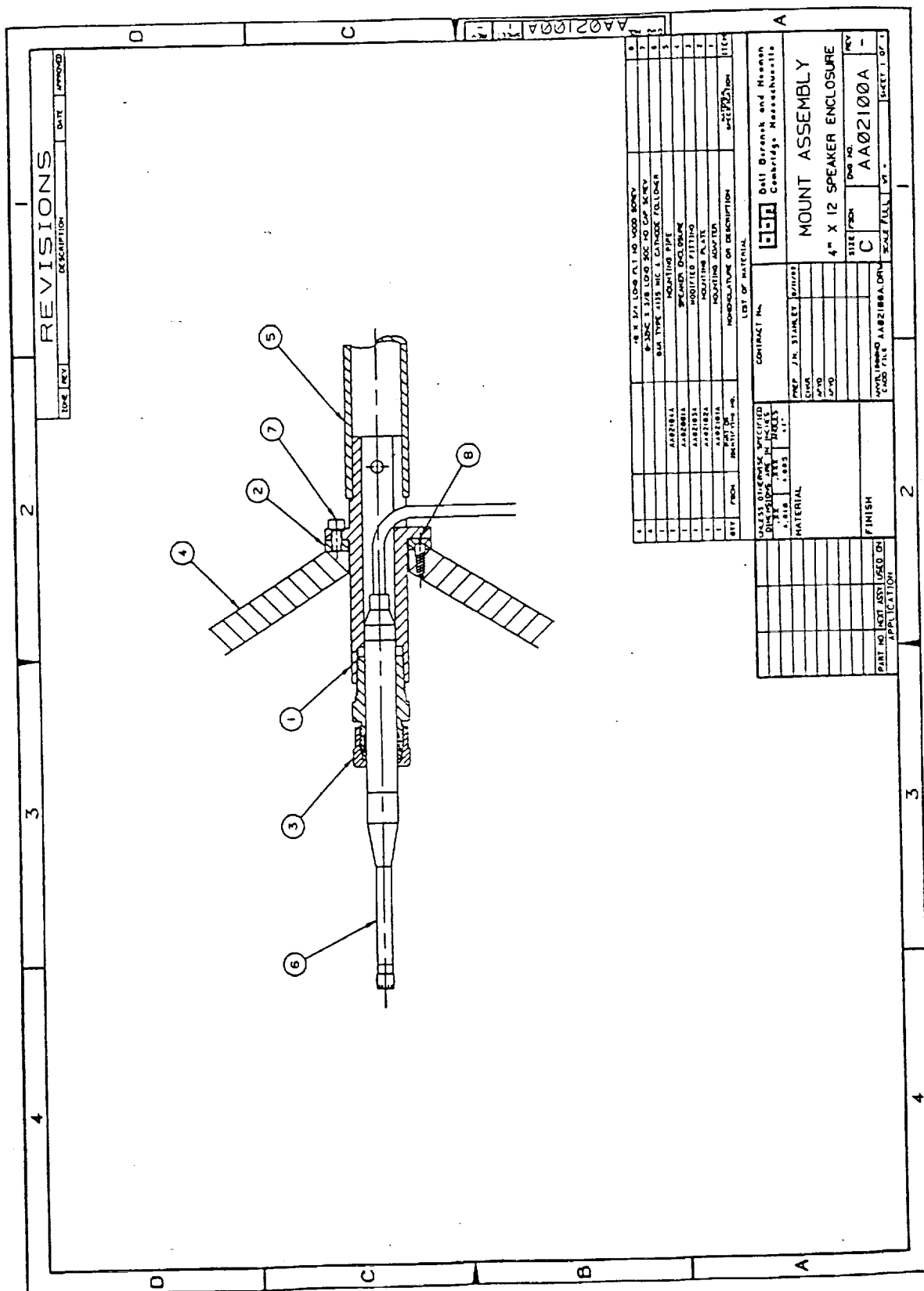
1. Rayleigh, Lord 1894 *The Theory of Sound*, Vol. 1, Chapter 5. London: Macmillan.
2. Lanczos, C. 1988 *Applied Analysis*. New York: Dover Publications.
3. Press, W. H., Flannery, B. P., Teukolsky, S. A. & Vetterling, W. T. 1986 *Numerical Recipes*. Cambridge University Press.

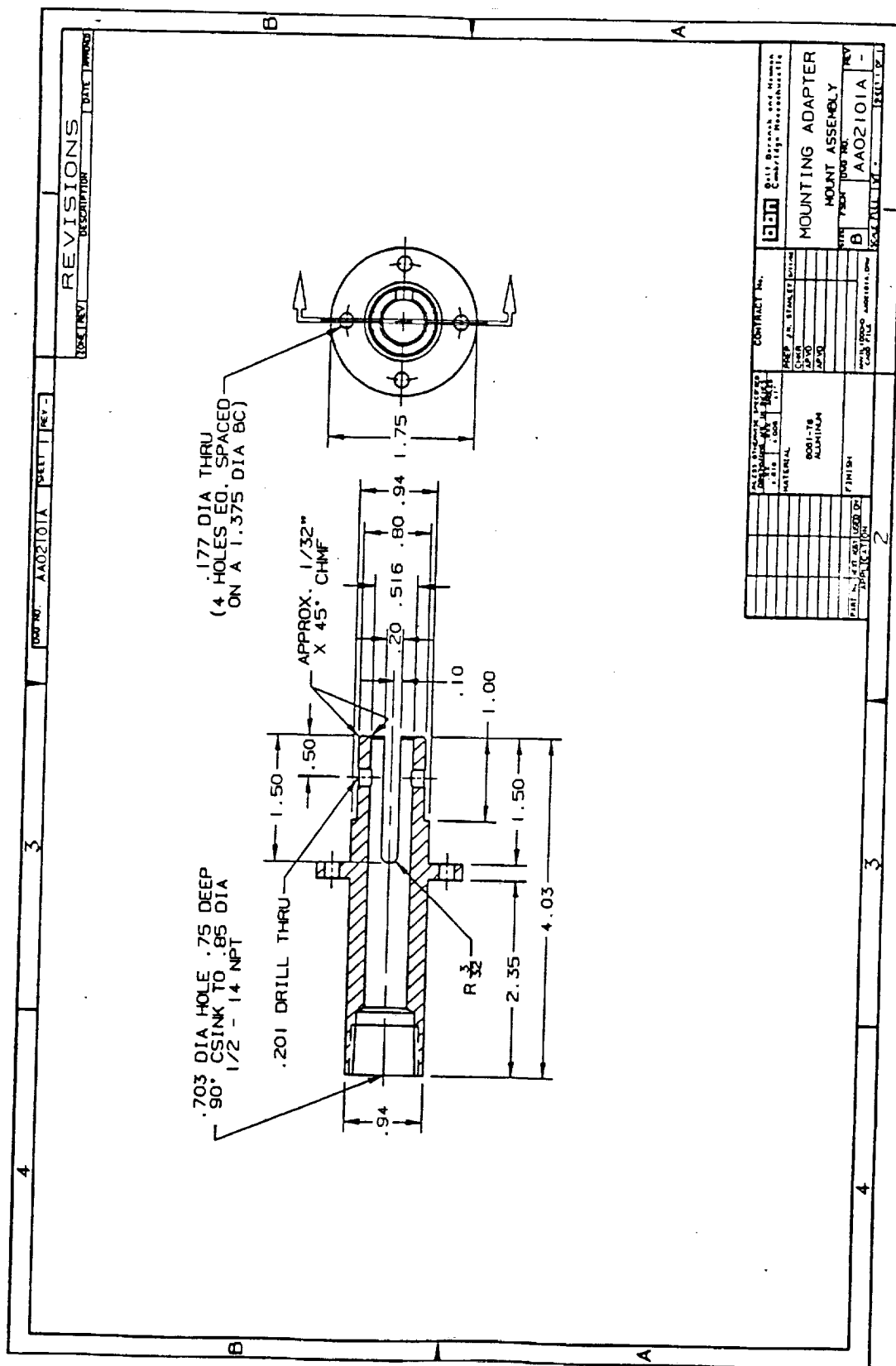
APPENDIX B

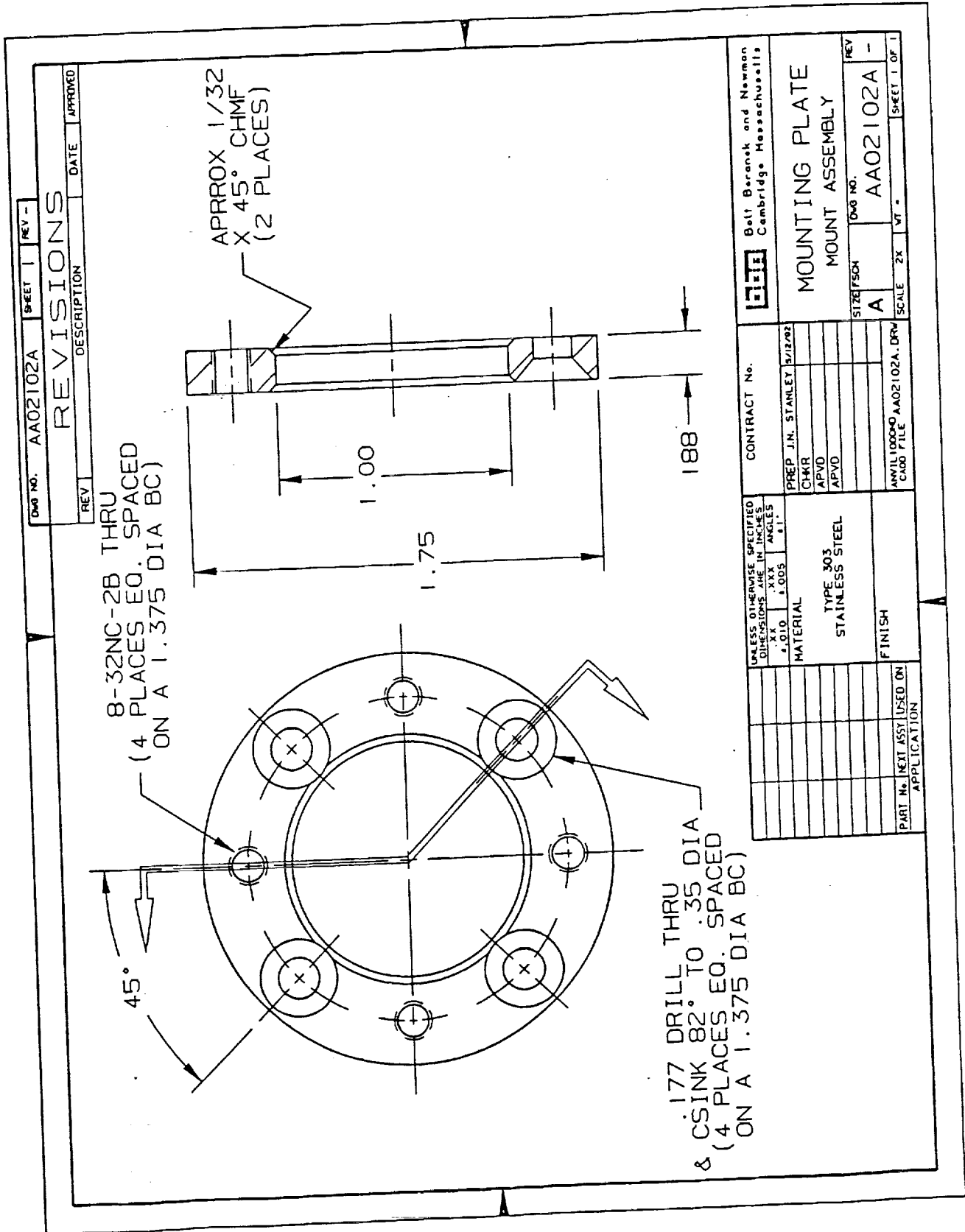
Construction Drawings for the  
Large Pentatondodecahedron Transducer













DWG NO. AA02103A	SHEET 1	REV -
REVISIONS		
REV	DESCRIPTION	DATE APPROVED

APPROX 1/32  
X 45° CHMF

.94 DIA

.505 ± .005

.94 DIA

UNLESS OTHERWISE SPECIFIED DIMENSIONS ARE IN INCHES FRACTIONS DECIMALS ANGLES 1/16 .015625 .001 1/16	CONTRACT No.	Bett Baronek and Newman Cambridge Massachusetts
MATERIAL	PREP J.N. STANLEY 5/12/02	MODIFIED FITTING MOUNT ASSEMBLY
CAJON 8-B-UT-1-B ULTRA-TOR MALE CONNECTOR	CHKR APVD APVD	SIZE/FSH A
FINISH	ANY/100000 AA02103A.DRW CADD FILE	DWG NO. AA02103A
PART No. NEXT ASSY USED ON APPLICATION	SCALE 2X	REV VT - SHEET 1 OF 1



APPENDIX C

Construction Drawings for the  
Small Pentatondodecahedron Transducer



[illegible]



